

We thank the reviewers for their comments. Our specific response can be found below. The reviewers' comments are in italics and changes made to the manuscript are in quotation marks. All the changes made do not affect the conclusions in the manuscript.

Response to Reviewer 1

The manuscript describes measurements of aerosol chemical composition at two sites in the greater London area. One site was located in a rural location, the other in an urban background location. The manuscript discusses differences in observed concentrations and composition between the two sites. It also evaluates results of measurements at the rural site using an Aerodyne thermodenuder (TD) to derive aerosol volatility and investigate how it depends on the O:C ratio. The manuscript has several weaknesses that need to be addressed prior to final acceptance. The main weakness concerns the treatment of aerosol volatility, which is given most attention in this review.

The key problem is the use of the (unfortunately) very popular mass fraction remaining (MFR). In this manuscript, and the authors are not alone in this approach, MFR is treated as if being identical in meaning to aerosol volatility. This is not correct. MFR is an extensive parameter, as it explicitly depends on aerosol mass concentration. On the other hand, aerosol volatility (saturation vapor concentration for pure compounds or a mole-fraction-averaged saturation concentration for compound mixtures) is an intensive parameter, which depends only on chemical nature of compounds in a mixture. Substituting one of these parameters for another leads to much confusion in this and many other papers on the subject. For example, this manuscript talks about OOA being less volatile than other OA fractions, which is true, but at a closer examination appears to be not as dramatic as it looks on MFR graphs. By observing an enrichment of OOA at higher temperatures, the authors seem to suggest that all low-volatility material is OOA, but that observation could be, at least partly, explained by the higher initial concentration of OOA (which is lost in the MFR representation). Differences in the initial concentration of OOA could also probably explain why O:C correlation with MFR-based "volatility" do not agree among different studies.

Below, I explain my point by using a back-of-the-envelope analysis. It is very simplistic, but does demonstrate the point. For the actual answers about the observed aerosol volatility, the authors should use kinetic modeling.

Let us begin with the fact that it is very unlikely that the aerosol was equilibrated in the TD used in this study. The characteristic time for aerosol equilibration is (Saleh et al. 2011): $\tau = 1 / (2\pi DN_p d_p F(d_p, \alpha))$, in which D is the species diffusion coefficient in the gas phase, N_p is particle number concentration, d_p is the particle size, $F(d_p, \alpha)$ is the Fuchs-Sutugin correction, and α is the accommodation coefficient. Assuming $d_p = 100$ nm and given that the aerosol volume concentration is about $10 \mu\text{m}^3/\text{cm}^3$, N_p would be of the order of 10^4 cm^{-3} . Making a generous assumption of $\alpha = 1$, the characteristic time is about 30 s. For a 200 nm aerosol, it will be about 2 times longer. It is more likely that α is of the order of 0.1 (Saleh et al., 2012, 2013), in which case the characteristic time will be about 10 times longer. In any case, the residence time of 5 s used in this study is (much) smaller than the characteristic time.

We should note that τ is the e-folding time, so at $t = \tau$ evaporation will proceed only about 30% towards equilibrium. At 5 s used in this study, equilibrium process is far from being completed, being actually just in its initial stages. This means the gas phase remains virtually unsaturated at the end of the TD and one can assume particles to be evaporating in a vapor-free environment. This allows us to make a back of the envelope approximation of saturation vapor concentration at the TD temperature for each of the factors (HOA, SFOA, OOA), see below.

Assuming vapor-free evaporation and making a first-order approximation of a constant particle size and $F = 1$, the change rate of aerosol concentration (C_a) is: $\frac{dC_a}{dt} \approx \frac{\bar{C}^}{\tau}$ in which \bar{C}^* is the mole-fraction-averaged saturation concentration, which for simplicity is assumed constant during evaporation (or one can use it as the evaporation-time-averaged saturation concentration). This can be easily integrated, such that a change in concentration after passage through the TD is: $\Delta C_a \approx \bar{C}^* * t_{res} / \tau$, where t_{res} is the residence time in the TD. Please note there are no MFRs in this above equation, only the absolute change in aerosol concentration. However, for our analysis, the key is that ΔC_a for each component is proportional to its \bar{C}^* ; the other parameters are the*

same for all the components. In other words, the ratio of ΔC of two compounds is equal to the ratio of their \overline{C} .

To estimate ΔC_a , we can use the reported MFRs, AND the initial aerosol concentrations ($\Delta C_a = C_{a,0}(1 - MFR)$). By using data from Fig.6 for the initial concentrations and Fig.9 for MFRs, I estimate that \overline{C} for OOA is within a factor of 2 of that of the other components. Yes, OOA is less volatile than the other two components, but the difference is less than one volatility bin in the traditional VBS representation (which is a factor of 10 in volatility space). In my opinion, the differences in volatilities between the three classes are minimal. This cannot be deduced from MFR alone, however. This also shows that making statements that OOA is the main contributor to the extremely low volatility compounds is not justified. For example, if there were 4 times more of HOA initially, there could be still a significant amount of HOA left after the TD. My point is that the presented data alone are not sufficient to make any conclusions about the contribution of OOA to the low volatility fraction.

The above analysis can also explain the “strange” dependence of MFR-based “volatility” on the O:C ratio, as well as discrepancies with other studies (unless MFR values are converted to more meaningful parameters). I do agree with the authors that distribution of O:C and individual factors over volatility bins needs to be known. But this can be achieved only using kinetic modeling, which has not been done in this study.

Thus, I suggest re-evaluating the data, preferably using a kinetic model to derive a VBS, though it may be difficult given only two temperature points have been measured.

As a side note, even if equilibrium is achieved, MFRs are still meaningless as can be easily demonstrated using a single component aerosol as an example – the same aerosol that has different initial concentrations will have different MFR “volatilities”, which is nonsense, of course. One should either derive a VBS or report OA mass loss data together with parameters of the size distribution and the residence time.

Response: We appreciate reviewer’s insightful suggestions/comments. The reviewer’s key points and our responses/changes are listed below.

(1) Relationship between mass fraction remaining (MFR) and volatility. We acknowledge that MFR is not equivalent to volatility. Thus, we have added the following discussions in the revised manuscript.

“The thermal denuder (TD) has been used widely to measure the aerosol volatility (An et al., 2007; Huffman et al., 2008; Saleh et al., 2011a). Many previous studies inferred the volatility from the mass fraction remaining (MFR) or volume fraction remaining (VFR), which is calculated as the ratio of the species mass (or volume) concentration after heating to an elevated temperature in the TD to the species mass (or volume) concentration without heating (An et al., 2007; Huffman et al., 2009b; Jonsson et al., 2007; Lee et al., 2011; Stanier et al., 2007; Grieshop et al., 2009b; Xu et al., 2014; Huffman et al., 2009a). Larger MFR is used as an indication for lower volatility of aerosol. However, Saleh et al. (2011b) suggested that it can be misleading to use MFR as an indication of volatility. This is mainly because the MFR is an extensive parameter (which explicitly depends on the initial mass concentration) while aerosol volatility is an intensive property (which depends only on chemical nature of the compounds in a mixture). Instead of MFR, Saleh et al. (2011b) presented that the change in mass concentration when reaching equilibrium upon heating (i.e., ΔC) is an appropriate measure of volatility.”

(2) Equilibrium timescale. With the reviewer’s suggestion, we calculate the characteristic time for aerosol equilibration in the TD by following the algorithm in Saleh et al. (2011). The characteristic time is about 1600s, which is orders of magnitude longer than that residence time (i.e., 5s) in the TD. Since the evaporation process is likely far away from equilibrium, we adopt the reviewer’s suggestion to use the change in concentration after heating in the TD (ΔC) to estimate volatility. We have modified the text in the revised manuscript.

“In this study, we calculate the characteristic time for aerosol equilibration by following the algorithm in Saleh et al. (2011b). To evaluate the equilibration time scale in the TD, the authors started with the mass transfer equation (Eq. (1)) and then obtained the characteristic time for aerosol equilibration (τ in Eq. (2)) by performing dimensional analysis.

$$\frac{dC_a}{dt} = -2\pi d_p D F N_{tot} (K C_{g,sat} - C_g) \quad \text{Eq. (1)}$$

$$\tau = \frac{1}{2\pi d_p D F N_{tot}} \quad \text{Eq. (2)}$$

$$F = \frac{1 + Kn}{1 + 0.3773Kn + 1.33Kn(1 + Kn) / \alpha} \quad \text{Eq. (3)}$$

In the equations, C_a , C_g , and $C_{g,sat}$ are the aerosol phase concentration, gas phase concentration, and gas phase saturation concentration, respectively. N_{tot} is the total number concentration, d_p is the particle size, D is the diffusion coefficient in the gas phase, K is the Kelvin effect correction, and F is the Fuchs-Sutugin correction, which is calculated by Eq. (3). In Eq. (3), Kn is the Knudsen number and α is the accommodation coefficient. D is on the order of $10^{-5} \text{ m}^2 \text{ s}^{-1}$ according to Tang et al. (2015) and α is on the order of 0.1 as shown in Saleh et al. (2011a). By using the campaign-average particle number concentration (i.e., $4.28 \times 10^3 \text{ cm}^{-3}$) and the mode of the particle number distribution (i.e., 87nm) in our study, we estimate that the characteristic equilibration time is about 1600s, which is orders of magnitude longer than that residence time (5s) in the TD. Since the evaporation process is likely far away from equilibrium, the gas phase saturation ratio is small and the particles are likely evaporating in a vapor-free environment. Under this assumption, the gas phase vapor concentration (i.e., C_g) in the mass transfer equation (Eq. (1)) can be neglected. After integration over the residence time in the TD, the change in mass concentration upon heating (ΔC_a) can be calculated by Eq. (4), in which $t_{residence}$ is the residence time in TD and the $\overline{C^*}$ is the evaporation-time-averaged saturation concentration. Thus, the ΔC_a for each component is proportional to its $\overline{C^*}$ because the other parameters are the same assuming the compounds are internally mixed.

$$\Delta C_a = C_{t=0} - C_{t_{residence}} = \int_0^{t_{residence}} \frac{KC_{g,sat}}{\tau} dt = \frac{t_{residence}}{\tau} K \overline{C^*} \quad \text{Eq. (4)}$$

By using this method, we find that the ΔC 's of three OA factors are not statistically different at 120°C. This suggests that although the O:C of OOA (O:C = 0.92) is substantially larger than that of HOA (O:C = 0.22) and SFOA (O:C = 0.37), the volatilities of the three factors are similar at 120°C. This is consistent with our conclusion that the average O:C may not be a good indicator of OA volatility. We have modified the manuscript accordingly.

(3) Statement that OOA is the main contributor to the extremely low volatility compounds. In the original manuscript, we only state that OOA is the main contributor to the residual OA at 250°C, instead of main contributor to the extremely low volatility compounds. For example, in the

conclusion part of our original manuscript, we stated that “We note that 16% of total OA remains even after heating at 250°C, suggesting the existence of non-volatile organics. PMF analysis reveals that the majority of the remaining organics are oxygenated OA.” Our statement is based on fig. 10, which clearly shows that the mass fraction of OOA in total PM₁ at 250°C is substantially larger than that of HOA and SFOA.

(4) Explanation for the “strange” relationship between MFR and O:C. While we cannot rule out the possibility that the difference in OA concentration between studies contribute to the various relationships between MFR and O:C, the distribution of O:C and volatility likely plays a more important role. For example, in Donahue et al. (2012), the O:C increases while the MFR decreases during the photochemical aging of α -pinene ozonolysis SOA. This anti-correlation between O:C and MFR cannot be explained by the dependence of MFR on OA concentration. This is because the OA concentration increases and the MFR decreases during the aging, which causes the ΔC to increase. The increase in both O:C and ΔC still indicates that the OA becomes more volatile as it is more oxidized.

We acknowledge that there are other possible explanations for the various relationship between O:C and MFR and we have added the following sentence.

“In addition to the distribution of O:C and volatility, the fact that MFR depends on the initial concentration of OA, which is different between studies, may also contribute to the various relationships between O:C and MFR.”

Other comments:

1. p. 23181, l.2. Even though the measurement setup at the urban site has been described elsewhere, it would be useful to have its brief description in this manuscript too.

Response: For the urban site, only the HR-ToF-AMS measurements are used in this study. We have added the following discussions in the revised manuscript.

“For instruments deployed at the urban NK site, only the high-resolution time-of-flight aerosol mass spectrometer (HR-ToF-AMS, Aerodyne) ambient measurements are included in this study. The data analysis of HR-ToF-AMS at the urban site is similar to that at the rural site, which will be discussed below. Details regarding the measurements at the NK site can be found in *Young et al. (2015a)*.”

2. p. 23181, l. 24. *Equilibrium does not depend on aerosol volatility (Saleh et al., 2011,2012). The references cited in the text used a wrong criterion for equilibration (Saleh et al., 2011).*

Response: We have modified the text and added Saleh et al., 2011 as a reference. The sentence now reads as the following.

“The time scale to reach thermodynamic equilibrium in a given TD depends on a number of factors, such as TD temperature, aerosol mass concentration, aerosol diameter, and mass accommodation coefficient (An et al., 2007; Riipinen et al., 2010; Saleh et al., 2011).”

3. p. 23182, 1st paragraph. *Equilibration time depends not only on aerosol concentration, but aerosol mean size and the accommodation coefficient (Saleh et al, 2011). Giving an equilibration time for an aerosol concentration without specifying the other two parameters is meaningless. As discussed above, it is very unlikely that equilibrium was achieved in the TD.*

Response: We have modified the discussion as shown above (i.e., the response to your major comment).

4. Section 2.3. *Much of the discussion of particle density derivation can be moved to the Supplement. I wonder how size changes upon evaporation affect the comparison between the derived and SMPS volumes. The SMPS measures up to 550 nm, while the optimal window for the AMS is between 100 - 500 nm, with larger sizes still contributing. Thus, a shift in size distribution could affect the intercomparison between different temperatures. I think the authors could also try to get a better insight into the BC density using SP2 and SP-AMS data: if a large fraction of BC particles was coated, the bulk density could be more appropriate.*

Response: Firstly, we thank the reviewer for this suggestion. However, we feel like that it is useful to include the discussion regarding the particle density in the main text. Importantly, the discussion highlights the uncertainties in AMS collection efficiency in TD measurements.

Secondly, we have checked the SMPS volume distribution under different TD temperatures. As shown in the figure R1, the mode in the volume distribution is 345, 290, and 290 nm for bypass line, TD 120°C, and TD 250°C, respectively. The volume distribution under three temperatures largely overlap the region where the AMS lens transmission efficiency is close to unity (Liu et al., 2007). Thus, the shift in size distribution does not affect the intercomparison.

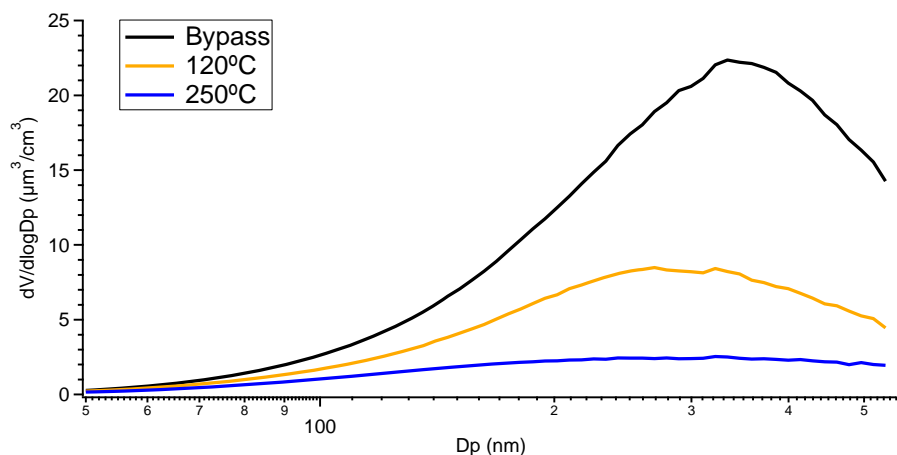


Figure R1. Campaign-average volume size distribution for bypass line, TD 120°C, and TD 250°C.

Thirdly, we also thank the reviewer’s suggestion regarding calculating the black carbon density based on the comparison between SP2 and SP-AMS. However, there are some uncertainties associated with this method, such as the shape factor of black carbon and the size distribution measured by SP2, which is beyond the scope of this manuscript. The BC particles get coated quickly in the atmosphere, therefore we use the bulk density for the bypass line. However, the BC coating is mostly removed in the TD after heating so that we use the effective density for the TD line.

5. Fig.S12 shows that the NO^+/NO_2^+ is 10-20% higher than for pure ammonium nitrate. What are the ratio values for organonitrates?

Response: The NO^+/NO_2^+ ratio of organic nitrate ranges from 5 to 10, which is about 2 – 4 times larger than that of ammonium nitrate. The 10-20% of the difference shown in Fig. S12 is likely within the uncertainty of the NO^+/NO_2^+ ratio of ammonium nitrate, which has been discussed in detail in a recent publication by Xu et al. (2015).

6. p.23190, l.18: Figure 4 is mentioned before Figure 3.

Response: Figure 3 (line 3) is introduced before figure 4 (line 18).

7. p.23193, 2nd paragraph. *The differences in sulfate concentration are troubling. If the differences in sulfate concentrations are observed mostly due to easterly flow, i.e. during long range transport, one has to wonder where does sulfate go during the transport over 45 km? Since easterly flows are associated with higher concentrations, one has to wonder about the instrument performance. A comparison between the two AMS-type instruments does not provide much insight, as both are essentially similar instruments.*

Response: Since submitting the manuscript, we continued to investigate the reason for the higher sulfate and OOA concentration at the rural Detling site. Based on the results from an atmospheric chemistry transport model (Ots et al., 2015), we find that the higher concentration at the rural site is a result of meteorological conditions, which cause a strong gradient of SOA concentration when air masses are advected from polluted mainland Europe.

Ots et al. (2015) applied the regional EMEP4UK (European Monitoring and Evaluation Programme) model, which uses 5 km by 5 km British Isles grid nested within 50 km by 50 km greater Europe domain, 21 vertical levels, Weather Research and Forecasting (WRF) model meteorological reanalysis, and National Atmospheric Emissions Inventory (NAEI) for the UK, Centre on Emission Inventories and Projections (CEIP) emissions for other European countries. The figure below shows the daily-averaged modelled SOA concentrations from Feb 4 to Feb 7. The white circles mark the urban NK site (left) and rural Detling site (right). They observed a steep negative gradient of SOA concentration from near European continent to southern England. The steep gradient is a result of meteorological conditions (i.e., mainly wind direction), which causes that the pollution plume from mainland Europe largely passes over the rural site, but not the urban site. This is consistent with our measurements. Detailed descriptions about the model and comparison between model and measurements can be found in Ots et al. (2015).

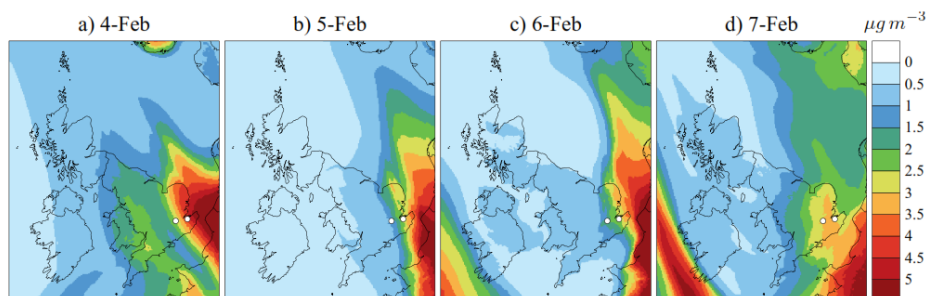


Figure R2. Modelled daily-average SOA concentration from Feb 4 to Feb 7, 2012. The white circles mark the urban NK site (left) and the rural Detling site (right). Adapted from Ots et al. (2015).

We have modified the text accordingly in the revised manuscript to discuss the results from Ots et al. (2015) and offer an explanation for higher sulfate and OOA concentration at the rural Detling site.

8. p.23193, 3rd paragraph. A more appropriate formulation would be “contribution of different sources is different” (the only source missing in Delting is cooking).

Response: We thank the reviewer for the suggestion. We have modified the text accordingly throughout the manuscript.

9. p.23197, 3rd paragraph. When discussing volatility of rBC coatings (Fig. 11), it would be more appropriate to compare the loss of mass from rBr with the bulk loss of mass.

Response: In the manuscript, we did not discuss the volatility of rBC coating. In figure 11, we compared the residual coating on rBC with residual bulk OA after heating to 250°C to provide insights about the sources of non-volatile organics.

10. p.23199 1st paragraph. *I cannot exclude the possibility of an external mixture in ambient aerosols and that it could explain some of the “strange” (from the MFR point of view) behavior with respect to the O:C ratio, but this argument does not hold for laboratory studies (such as smog chamber studies), where aerosol is most probably internally mixed. In addition to the issues associated with the use of MFR, O:C ratio’s connection to volatility is quite tenuous anyway. Yes, addition of an oxygenated group to a molecule significantly reduces its volatility. On the other hand, taking dicarboxylic acids as an example, volatility decreases 3-4 orders of magnitude from oxalic acid to azelaic acid, while the O:C decreases from 2 to 0.44 thus showing an opposite trend. This demonstrates that using O:C as a surrogate for volatility is always going to be quite problematic unless other parameters (such as the carbon chain length) are taken into account.*

Response: We propose that the distribution of O:C is one possible explanation for the various relationships between MFR and average O:C of bulk OA. The explanation proposed by the reviewer has been incorporated in the revised manuscript. We refer the reviewer to the response to your major comment.

Response to Reviewer 2

1. *Although the authors performed retroplume analysis, inclusion of wind direction would be helpful, at least a wind rose plot showing the prevailing wind during this study.*

Response: We have added the wind rose plot in the revised supplemental information (Figure S1(b)).

2. *The average wind speed was 5.8 m s^{-1} , and the distance between the two sites is 45 km. This means that the transport time from the urban site to the rural site was generally within 2 hours. Could the authors explain how biomass burning aerosol can be rapidly oxidized to OOA in such a short time in winter when photochemical processing is often weak?*

Response: In this study, most of the air masses are easterly (i.e., mainland Europe), so we did not sample the urban outflow from London. Based on the results from an atmospheric chemistry transport model (Ots et al., 2015), the higher OOA concentration at the rural site is a result of meteorological conditions, which cause a strong gradient of SOA concentration when air masses are advected from polluted mainland Europe. We refer the reviewer to the response to comment #7 of reviewer #1.

3. Page 23816, line 10, no Eq. (4).

Response: Thanks for the note. We have deleted “Eq. (4)” in the sentence.

4. The OA fraction of the campaign average at the Detling site was the same in Figure 3 and Figure 6. Could it be some mistake since the organics loading and the period for the calculation was different.

Response: This is just a coincidence. The mass fractions are different if using three significant digits. For example, the mass fraction of HOA at the Detling site is 19.3% in figure 3 (average of the whole campaign period) and 18.6% in figure 6 (average for periods when instruments at both sites were operative).

5. I am thinking if it is appropriate to connect the three points using straight lines in Figure 9 since the relationship is not linear.

Response: The points are connected by lines to guide the eyes. We have added this in the figure caption.

6. Change “(b)” to “(b – e)” in the caption of Figure 12.

Response: We have modified the caption accordingly.

References

Donahue, N. M., Henry, K. M., Mentel, T. F., Kiendler-Scharr, A., Spindler, C., Bohn, B., Brauers, T., Dorn, H. P., Fuchs, H., Tillmann, R., Wahner, A., Saathoff, H., Naumann, K. H., Mohler, O., Leisner, T., Müller, L., Reinnig, M. C., Hoffmann, T., Salo, K., Hallquist, M., Frosch, M., Bilde, M., Tritscher, T., Barmet, P., Praplan, A. P., DeCarlo, P. F., Dommen, J., Prevot, A. S. H., and Baltensperger, U.: Aging of biogenic secondary organic aerosol via gas-phase OH radical reactions, *P Natl Acad Sci USA*, 109, 13503-13508, DOI 10.1073/pnas.1115186109, 2012.

Liu, P. S. K., Deng, R., Smith, K. A., Williams, L. R., Jayne, J. T., Canagaratna, M. R., Moore, K., Onasch, T. B., Worsnop, D. R., and Deshler, T.: Transmission efficiency of an aerodynamic focusing lens system: Comparison of model calculations and laboratory measurements for the Aerodyne Aerosol Mass Spectrometer, *Aerosol Sci Tech*, 41, 721-733, Doi 10.1080/02786820701422278, 2007.

Ots, R., Young, D. E., Vieno, M., Xu, L., Dunmore, R. E., Allan, J. D., Coe, H., Williams, L. R., Herndon, S. C., Ng, N. L., Hamilton, J. F., Bergström, R., Marco, C. D., Nemitz, E., Mackenzie, I. A., Kuenen, J. J. P., Green, D. C., Reis, S., and Heal, M. R. H.: Simulating secondary organic aerosol from missing diesel-related intermediate-volatility organic compound emissions during the Clean Air for London (ClearLo) campaign, Submitted to Atmos. Chem. Phys. , 2015.

Saleh, R., Shihadeh, A., and Khlystov, A.: On transport phenomena and equilibration time scales in thermodenuders, Atmos. Meas. Tech., 4, 571-581, 10.5194/amt-4-571-2011, 2011.

Xu, L., Suresh, S., Guo, H., Weber, R. J., and Ng, N. L.: Aerosol characterization over the southeastern United States using high-resolution aerosol mass spectrometry: spatial and seasonal variation of aerosol composition and sources with a focus on organic nitrates, Atmos. Chem. Phys., 15, 7307-7336, 10.5194/acp-15-7307-2015, 2015.

Wintertime aerosol chemical composition, volatility, and spatial variability in the greater London area

L. Xu¹, L.R. Williams², D.E. Young^{3,*}, J.D. Allan^{3,4}, H. Coe³, P. Massoli², E. Fortner², P. Chhabra^{2,**}, S. Herndon², W.A. Brooks², J.T. Jayne², D.R. Worsnop², A.C. Aiken⁵, S. Liu^{5,***}, K. Gorkowski^{5,****}, M.K. Dubey⁵, Z.L. Fleming^{6,7}, S. Visser⁸, A.S.H. Prevot⁸, N.L. Ng^{1,9}

¹School of Chemical and Biomolecular Engineering, Georgia Institute of Technology, Atlanta, GA, USA

²Aerodyne Research Inc., Billerica, MA, USA

³School of Earth, Atmospheric and Environmental Sciences, University of Manchester, Manchester, UK

⁴National Centre for Atmospheric Science, University of Manchester, Manchester, UK

⁵Earth and Environmental Sciences Division, Los Alamos National Laboratory, Los Alamos, New Mexico, USA.

⁶Department of Chemistry, University of Leicester, Leicester UK

⁷National Centre for Atmospheric Science, University of Leicester, Leicester, UK

⁸Laboratory of Atmospheric Chemistry, Paul Scherrer Institute, Villigen, Switzerland

⁹School of Earth and Atmospheric Sciences, Georgia Institute of Technology, Atlanta, GA, USA

*now at: Department of Environmental Toxicology, University of California, Davis, CA, USA

**now at: PerkinElmer Inc. Hopkinton, MA

***now at: Cooperative Institute for Research in the Environmental Sciences, University of Colorado, Boulder, Colorado, USA.

****now at: ~~Civil and Environmental Engineer Department~~[Center for Atmospheric Particle Studies](#), Carnegie Mellon University, Pittsburgh, PA, USA

Correspondence to N. L. Ng (ng@chbe.gatech.edu)

Abstract

The composition of PM₁ (particulate matter with diameter less than 1 μm) in the greater London area was characterized during the Clean Air for London (ClearLo) project in winter 2012. Two High-Resolution Time-of-Flight Aerosol Mass Spectrometers (HR-ToF-AMS) were deployed at a rural site (Detling, Kent) and an urban site (North Kensington, London). The simultaneous and high-temporal resolution measurements at the two sites provide a unique opportunity to investigate the spatial distribution of PM₁. We find that the organic aerosol (OA) concentration is comparable between the rural and urban sites, but the contribution from different sources of OA are distinctly different between the two sites. The concentration of solid fuel OA at the urban site is about twice as high as at the rural site, due to elevated domestic heating in the urban area. While the concentrations of oxygenated OA (OOA) are well-correlated between the two sites, the OOA concentration at the rural site is almost twice that of the urban site. At the rural site, more than 70% of the carbon in OOA is estimated to be non-fossil, which suggests that OOA is likely related to aged biomass burning considering the small amount of biogenic SOA in winter. Thus, it is possible that the biomass burning OA contributes a larger fraction of ambient OA in wintertime than what previous field studies have suggested.

A suite of instruments was deployed downstream of a thermal denuder (TD) to investigate the volatility of PM₁ species at the rural Detling site. After heating at 250°C in the TD, 40% of the residual mass is OA, indicating the presence of non-volatile organics in the aerosol. Although the OA associated with refractory black carbon (rBC, measured by a soot-particle aerosol mass spectrometer) only accounts for <10% of the total OA (measured by a HR-ToF-AMS) at 250°C, the two measurements are well-correlated, suggesting that the non-volatile organics have similar sources or have undergone similar chemical processing as rBC in the atmosphere. Although the atomic O:C ratio of OOA is substantially larger than that of solid fuel OA and hydrocarbon-like OA, these three factors have similar volatility, which is inferred from the change in mass concentration after heating at 120°C. Finally, we discuss the relationship between the mass fraction remaining (MFR) of OA volatility after heating in the TD and atomic O:C of OA and find that particles with a wide range of O:C could have similar mass fraction remaining-MFR after heating. This analysis emphasizes the importance of understanding the distribution of volatility and O:C in bulk OA.

Formatted: Font color: Auto

Formatted: Font color: Auto

Formatted: Font color: Auto

Formatted: Font color: Auto

Formatted: Font color: Auto

Formatted: Font color: Auto

Formatted: Font color: Auto

Formatted: Font color: Auto

Formatted: Font color: Auto

1 Introduction

Particulate matter (PM) concentration in the greater London area often exceeds European air quality limits, causing adverse effects on the health of habitants in this area (Harrison et al., 2012; Bohnenstengel et al., 2014). Therefore, it is critical to identify the PM sources in order to implement effective strategies to control ambient pollutants. The Clean Air for London (ClearfLo) project aimed to study boundary layer pollution in the greater London area through comprehensive measurements of meteorology, gaseous and particulate composition (Bohnenstengel et al., 2014). Multiple monitoring sites were set up in both urban and rural areas around London to quantify the urban increment in gas-phase and particle-phase pollutants.

Previous studies in the greater London area have repeatedly shown that the concentration of elemental carbon (EC) is higher in urban sites than rural sites due to elevated levels of primary emissions such as vehicle exhaust and wood smoke (Crilley et al., 2015; Yin et al., 2015). The origin of organic carbon (OC) at urban and rural sites is instead more challenging to elucidate considering the myriad of different OC sources. Based on the ratios among multiple tracers (e.g., EC/OC and levoglucosan/OC) from different sources, Crilley et al. (2015) estimated that the concentration of primary OC from vehicle emissions was higher in an urban area compared to a rural area in the UK. Many studies have applied the Chemical Mass Balance (CMB) model for OC apportionment (Yin et al., 2010; Crilley et al., 2015; Yin et al., 2015). However, due to the uncertainties in the source profiles and the number of organic tracers included in the model, the concentration of secondary OC is highly uncertain. In addition, OC measurements based on filter samples on a daily basis limit the temporal resolution of rural vs. urban comparisons.

Factor analysis via Positive Matrix factorization (PMF) of aerosol mass spectrometer (AMS) measurements is another widely used method to identify sources of organic aerosol (OA) (Jimenez et al., 2009; Lanz et al., 2007; Ng et al., 2010; Xu et al., 2015a). Based on factor analysis of AMS measurements around the world, Zhang et al. (2007) observed that the contribution of hydrocarbon-like OA (a surrogate for primary OA) to total OA decreased from urban sites to rural sites, but the oxygenated OA (a surrogate for secondary OA), showed the opposite trend. The authors also showed that the average OA concentration is substantially lower in rural sites than urban sites (2.8 vs. 7.6 $\mu\text{g m}^{-3}$). However, the trend observed in Zhang et al. (2007) needs to be

further verified since the urban vs. rural comparisons are not based on simultaneous measurements between paired locations.

Comparison based on simultaneous measurements between different sites, especially between rural and urban sites, is useful to identify regional and local sources of OA. For example, by comparing concurrent AMS measurements of OA at multiple sites in the greater Atlanta area, USA, Xu et al. (2015b) showed that the OA was spatially homogeneous and mainly regional in summer, but the OA showed ~~substantially~~substantial spatial variability in winter. Based on PMF analysis of AMS measurements, Crippa et al. (2013) investigated the correlation of various OA subtypes between three urban sites located in a 20km-radius region in Paris, France during winter 2010. The authors observed that the secondary OA factor had substantially better correlation between different sites than the primary OA factors, including OA from vehicle, biomass burning, and cooking. However, a rural vs. urban comparison was not performed in Crippa et al. (2013).

In addition to OA sources, the volatility of OA is an important property since it directly determines the gas/particle partitioning. ~~Multiple~~The thermal denuder (TD) has been used widely to measure the aerosol volatility (An et al., 2007; Huffman et al., 2008; Saleh et al., 2011a). Many previous studies inferred the volatility from the mass fraction remaining (MFR) or volume fraction remaining (VFR), which is calculated as the ratio of the species mass (or volume) concentration after heating to an elevated temperature in the TD to the species mass (or volume) concentration without heating (An et al., 2007; Huffman et al., 2009b; Jonsson et al., 2007; Lee et al., 2011; Stanier et al., 2007; Grieshop et al., 2009b; Xu et al., 2014; Huffman et al., 2009a). Larger MFR is used as an indication for lower volatility of aerosol. However, Saleh et al. (2011b) suggested that it is misleading to use MFR as an indication of volatility. This is mainly because the MFR is an extensive parameter (which explicitly depends on the initial mass concentration) while aerosol volatility is an intensive property (which depends only on chemical nature of the compounds in a mixture). Instead of MFR, Saleh et al. (2011b) presented that that change in mass concentration when reaching equilibrium upon heating (i.e., ΔC) is an appropriate measure of volatility.

Although multiple previous studies have investigated the volatility of laboratory-generated OA (An et al., 2007; Huffman et al., 2009b; Jonsson et al., 2007; Lee et al., 2011; Stanier et al., 2007; Grieshop et al., 2009b; Xu et al., 2014), ~~but~~ there are only limited studies on the volatility of ambient OA, especially on the volatility of OA from different sources (Hildebrandt et al., 2010;

Formatted: Font color: Auto

Huffman et al., 2009a; Massoli et al., 2015; Paciga et al., 2015). Previous studies have showed the presence of non-volatile organics in the ambient aerosol even after heating to high temperatures (i.e., 230 - 300°C) (Huffman et al., 2009a; Häkkinen et al., 2012; Poulain et al., 2014; Massoli et al., 2015; Liu et al., 2015). However, the sources of non-volatile organics are uncertain. Häkkinen et al. (2012) and Poulain et al. (2014) found that the non-volatile residuals correlated with anthropogenic tracers, such as BC and polycyclic aromatic hydrocarbons (PAHs), implying that the non-volatile species are possibly linked to anthropogenic emissions. However, in both studies, the thermal-denuder (TD) was only applied upstream of a scanning mobility particle sizer (SMPS); therefore the composition of remaining compounds ~~cannot be~~ was not directly measured but only conjectured. Massoli et al. (2015) coupled a TD with a soot-particle AMS (SP-AMS) during measurements in California. The authors observed the existence of refractory OA (i.e., detectable via laser vaporization in the SP-AMS, but not detectable by vaporization at 600°C in the standard AMS), which was present in the fresh urban air masses, but not in the aged air masses.

~~The~~ Many studies have used the degree of oxidation of OA, such as atomic O:C ratio and oxidation state (OS), ~~is generally thought to be~~ as a proxy for volatility. For example, two oxygenated OA factors with high but different O:C ratio are often resolved from PMF analysis on AMS data. These two oxygenated OA factors are often named semi-volatile OOA (~~i.e.~~, SVOOA) and low-volatility OOA (~~i.e.~~, LVOOA) based on the ~~inferred~~ volatility inferred from O:C values (Ng et al., 2010; Huang et al., 2010; Mohr et al., 2012; Jimenez et al., 2009). In a laboratory study on toluene SOA, Hildebrandt Ruiz et al. (2014) observed a linear relationship between OS and effective saturation concentration of the aerosol. However, for both ambient measurements and laboratory studies, it is uncertain whether the O:C or OS of bulk OA is a good indicator of volatility (~~usually inferred based on mass or volume fraction remaining after heating in a TD~~). In Mexico City and Riverside, CA, Huffman et al. (2009a) showed that the O:C ratio of the thermally-denuded OA increased with TD heating temperature, which suggests that the O:C is inversely correlated with the volatility of organic aerosol (i.e., higher O:C indicates the residual OA with lower volatility ~~and higher mass fraction remaining~~ after heating has a higher O:C). In contrast, only a weak correlation between O:C and volatility was observed in Hildebrandt et al. (2010), who measured the volatility of ambient OA in Finokalia, Greece. The authors found that between thermally-denuded OA and ambient OA, the mass spectrum was similar and the difference in f_{44} (i.e., fraction of organic signal at m/z 44, which has a linear correlation with O:C) was not

Formatted: Font color: Auto

Formatted: Font color: Auto

Formatted: Font color: Auto

Formatted: Font color: Auto

Formatted: Font color: Auto

Formatted: Font color: Auto

statistically significant. This indicates that the degree of oxidation does not change after evaporation of relatively volatile species. ~~In laboratory studies, the relationship~~ ~~relationships~~ ~~between O:C and volatility~~ ~~also varies for~~ ~~(inferred from the MFR)~~ ~~have been~~ ~~observed in previous laboratory studies on~~ different SOA systems (Grieshop et al., 2009b; Qi et al., 2010; Donahue et al., 2012; Kroll et al., 2009; Tritscher et al., 2011; Xu et al., 2014). For example, Xu et al. (2014) observed that while the O:C of isoprene SOA formed in the laboratory without additional NO remained fairly constant (~0.6) during photochemical aging, ~~the SOA became less volatile over time (i.e., volume fraction remaining increases).~~ ~~VFR increased over time,~~ Grieshop et al. (2009b) showed that during photochemical aging, OA from wood fires became more oxidized (i.e., O:C increases), but the ~~volatility~~ ~~MFR~~ remained constant. Donahue et al. (2012) studied the photochemical aging of α -pinene ozonolysis SOA and observed that while the OA became more oxidized, ~~it became more volatile~~ ~~(i.e., volume fraction remaining decreases)~~ ~~O:C increases~~, the VFR decreased with aging. The authors proposed that the photochemical aging produced both relatively volatile products and more oxidized products, which broadened the volatility distribution of the OA (Donahue et al., 2012). In ~~brief summary~~, while ~~the~~ SOA becomes progressively more oxidized (i.e., O:C increases) during ~~chemical~~ aging, the ~~mass fraction remaining (MFR)~~ ~~or VFR~~ exhibits different trends (i.e., increases, stays constant, or decreases over time) for different SOA systems.

In this study, we performed simultaneous measurements at a rural site (Detling, Kent) and an urban site (North Kensington, London) in the greater London area in winter 2012 using two Aerodyne high resolution time-of-flight mass spectrometers (HR-ToF-AMS) (DeCarlo et al., 2006). The comparison of the simultaneous, high temporal resolution measurements and the OA source apportionment by PMF analysis provide insights into sources of wintertime OA in the greater London area. Since biogenic emissions are low in winter, these measurements allow a more direct evaluation of the contributions of anthropogenic emissions to OA formation. We also deployed a thermal denuder upstream of a suite of instruments to directly characterize the non-volatile residual at 250°C. Furthermore, we investigated the volatility of different OA sources and systematically evaluated the relationship between O:C and OA volatility.

- Formatted: Font color: Auto
- Formatted: Font color: Auto
- Formatted: Font color: Auto
- Field Code Changed
- Formatted: Font color: Auto
- Formatted: Font color: Auto
- Formatted: Font color: Auto
- Field Code Changed
- Formatted: Font color: Auto
- Formatted: Font color: Auto
- Formatted: Font color: Auto
- Field Code Changed
- Formatted: Font color: Auto
- Formatted: Font color: Auto
- Formatted: Font color: Auto
- Formatted: Font color: Auto

2 Method

2.1 Sampling sites and meteorological conditions

Measurements were performed as part of the Clean Air for London (ClearfLo) project. An overview of the ClearfLo field campaign can be found in Bohnenstengel et al. (2014). The main goal of the ClearfLo project was to study boundary layer pollution in the greater London area by comprehensive measurements of meteorology, gaseous- and particulate composition. Multiple monitoring sites were set up in both urban and rural areas and at different elevations (street and elevated level) to perform year-long measurements across London. In addition, two intensive observation periods (IOPs) were conducted during winter (January-February, 2012) and summer (July-August, 2012). Data presented in this paper were collected at the Detling site and the North Kensington (NK) site during the winter IOP. Figure 1 shows the locations of both sites. The NK site (51.521055°N, 0.213432°W) is an urban background site located in a residential area, 7 km to the west of central London. The Detling site (51.301931°N, 0.589494°E) is a rural site located on a plateau (200 m a.s.l.), 45 km southeast of London. The closest road is about 150m (south), which carries ~42,000 vehicles per day (www.dft.gov.uk/traffic-counts). The typical meteorological data (temperature, relative humidity, and wind speed) at the Detling site are shown in Fig. S1a. The campaign-average temperature ~~is was~~ 6°C. In the diurnal variation, the highest temperature ~~is was~~ ~8°C at 14:00 and the lowest temperature ~~is was~~ ~5°C at 7:00. ~~The relative humidity was 83% on average.~~ The wind speed ~~is was~~ 5.8 m s⁻¹ on average, but it ~~reaches~~reached 10 m s⁻¹ occasionally. ~~The relative humidity is 83% on average. The wind rose plot is shown in Fig. S1b. The prevailing wind was from the northeast and the southwest.~~

2.2 Instrumentation

In the following discussions on instrumental setup and data analysis methods, we ~~will~~ focus on the rural Detling site. ~~as the details. For instruments deployed at the urban NK site, only the high-resolution time-of-flight aerosol mass spectrometer (HR-ToF-AMS, Aerodyne) ambient measurements are included in this study. The data analysis of HR-ToF-AMS at the urban site is similar to that at the rural site, which will be discussed below. Details regarding the measurements at the NK site have been discussed~~ can be found in Young et al. (2015a).

Formatted: Font color: Auto

Formatted: Font color: Auto

Formatted: Font color: Auto

Field Code Changed

Formatted: Font color: Auto

Formatted: Font color: Auto

A suite of instruments was deployed at the Detling site to characterize both the gas-phase and particle-phase composition. Instruments of interest to this study are shown in Fig. S2 and are described below. Ambient particles were sampled through a PM_{2.5} cyclone and then directed through either a thermal denuder (denoted as TD line) or bypass line (denoted as bypass line) before being analyzed by downstream instruments. The thermal denuder (TD, Aerodyne), designed based on Huffman et al. (2008), consists of a 22” long stainless steel tube operated at elevated temperatures (i.e., heated section), followed by a 24” section of activated charcoal held at room temperature to adsorb the evaporated components from particles. The heating section was operated at 120 and 250°C. The aerosol residence time in the heating section of the TD was 5.3 s at the experimental flowrate rate (2.3 LPM determined by the sampling rate of instruments downstream of the TD). Caution is required when comparing the results between different studies with a TD because the TD configuration and residence times can be different. Particle loss in the TD was characterized based on the single particle soot photometer (SP2) refractory black carbon (rBC) mass measurement during the field campaign, since rBC does not evaporate even at 250°C. The transmission efficiency of TD is about 90% (Fig. S3), similar to the values reported in previous studies with similar TD configurations (Huffman et al., 2008; Massoli et al., 2015). The time scale to reach thermodynamic equilibrium in a given TD depends on a number of factors, such as TD temperature, aerosol mass concentration, aerosol diameter, ~~aerosol volatility,~~ and mass accommodation coefficient (Riipinen et al., 2010; An et al., 2007; Saleh et al., 2011b). ~~Riipinen et al. (2010) developed a mass transfer model and estimated that the equilibrium time spanned from seconds to hours depending on the factors mentioned above. The authors also showed that the equilibrium time decreased with increasing TD temperature. For example, they estimated that it required about 10s to reach equilibrium at 200°C when the OA concentration was 5 µg m⁻³. In this study, although the residence time in the heating section of TD (i.e., 5.3s) was shorter than 10s, the temperature of interest (i.e., 250°C) was higher than 200°C. Thus, major kinetic limitations were likely avoided. In this study, we calculate the characteristic time for aerosol equilibration by following the algorithm in Saleh et al. (2011b). To evaluate the equilibration time scale in the TD, the authors started with the mass transfer equation (Eq. (1)) and then obtained the characteristic time for aerosol equilibration (τ in Eq. (2)) by performing dimensional analysis.~~

$$\frac{dC_a}{dt} = -2\pi d_p D F N_{tot} (K C_{g,sat} - C_g) \quad \text{Eq. (1)}$$

Formatted: Indent: First line: 0.5"

Field Code Changed

Formatted: Font color: Auto

Formatted: Font color: Auto

$$\tau = \frac{1}{2\pi d_p D F N_{tot}} \quad \text{Eq. (2)}$$

$$F = \frac{1 + Kn}{1 + 0.3773Kn + 1.33Kn(1 + Kn) / \alpha} \quad \text{Eq. (3)}$$

In the equations, C_a , C_g , and $C_{g,sat}$ are the aerosol phase concentration, gas phase concentration, and gas phase saturation concentration, respectively. N_{tot} is the total number concentration, d_p is the particle size, D is the diffusion coefficient in the gas phase, K is the Kelvin effect correction, and F is the Fuchs-Sutugin correction, which is calculated by Eq. (3). In Eq. (3), Kn is the Knudsen number and α is the accommodation coefficient. D is on the order of $10^{-5} \text{ m}^2 \text{ s}^{-1}$ according to Tang et al. (2015) and α is on the order of 0.1 as shown in Saleh et al. (2011a). By using the campaign-average particle number concentration (i.e., $4.28 \times 10^3 \text{ cm}^{-3}$) and the mode of the particle number distribution (i.e., 87nm) in our study, we estimate that the characteristic equilibration time is about 1600s, which is orders of magnitude longer than that residence time (5s) in the TD. Since the evaporation process is likely far away from equilibrium, the gas phase saturation ratio is small and the particles are likely evaporating in a vapor-free environment. Under this assumption, the gas phase vapor concentration (i.e., C_g) in the mass transfer equation (Eq. (1)) can be neglected. After integration over the residence time in the TD, the change in mass concentration upon heating (ΔC_a) can be calculated by Eq. (4), in which $t_{residence}$ is the residence time in TD and the \bar{C}^* is the evaporation-time-averaged saturation concentration. Thus, the ΔC_a for each component is proportional to its \bar{C}^* because the other parameters are the same assuming the compounds are internally mixed.

$$\Delta C_a = C_{t=0} - C_{t_{residence}} = \int_0^{t_{residence}} \frac{KC_{g,sat}}{\tau} dt = \frac{t_{residence}}{\tau} K \bar{C}^* \quad \text{Eq. (4)}$$

A high-resolution time-of-flight aerosol mass spectrometer (HR-ToF-AMS, Aerodyne), a soot-particle aerosol mass spectrometer (SP-AMS, Aerodyne), a single particle soot photometer (SP2, DMT), and a scanning mobility particle sizer (SMPS, TSI) were placed downstream of the TD. These four instruments alternated between sampling the bypass line (i.e., ambient) and the TD line (i.e., thermally-denuded) every 10 min. When the instruments were sampling through the

bypass line, the heating section of TD was adjusted to the subsequent temperature setpoint. The MFR was determined by comparing the measurements between bypass line and TD line.

The HR-ToF-AMS provides real-time measurements of the chemical composition and size distribution of submicron non-refractory species (NR-PM₁) and has been described in detail previously (Canagaratna et al., 2007; DeCarlo et al., 2006). In brief, the HR-ToF-AMS samples particles through an aerodynamic lens and then impacts the focused particle beam on a heated tungsten surface (~600°C). The resultant vapors are ionized by electron impact ionization and the ions are analyzed using time-of-flight mass spectrometry. We used the ambient gas-phase CO₂ concentration (measured by a LI-COR CO₂ gas analyzer with 1 min resolution) to correct for the gas-phase interference in the particle-phase CO₂⁺ signals for both the bypass line and TD line. The assumption behind this correction for the TD line is that the CO₂ generated in the TD, if it exists, is negligible. Unless otherwise specified, the elemental ratios, such as atomic O:C and H:C, were calculated based on the latest recommendation by Canagaratna et al. (2015), who modified the original method developed for the HR-ToF-AMS (Aiken et al., 2007; Aiken et al., 2008). The HR-ToF-AMS data were analyzed using the standard AMS analysis toolkits SQUIRREL v1.56A and PIKA v1.15.

The SP-AMS measures the chemical composition of rBC containing particles by using an intracavity laser vaporizer (1064 nm). The detailed working principles of SP-AMS are extensively discussed in Onasch et al. (2012). In brief, after being focused through an aerodynamic lens, the rBC-containing particles are heated and vaporized by laser absorption. The chemical composition of both the rBC and any associated coatings are analyzed via high-resolution mass spectrometry. The SP-AMS data presented in this paper were obtained between 5 and 15 February, 2012, when the instrument was operated in the laser vaporizer only configuration, that is, only rBC-associated species were detected. Analysis and interpretation of the SP-AMS measurements for the entire deployment at Detling are presented in Williams et al. (2015).

The single particle soot photometer (SP2) measures rBC using laser-induced incandescence. The method has been described previously (Schwarz et al., 2006; Stephens et al., 2003). In brief, a 1064 nm Nd:YAG laser irradiates the particles as they enter the SP2, where upon vaporization and incandescence is induced in the particles containing rBC. The incandescence signal is proportional to the mass of rBC per particle, and with the sampling volume, rBC mass

concentrations are quantified. The SP2 at the Detling site was calibrated using fullerene soot (Alfa Aesar, Inc., Ward Hill, Massachusetts; Stock# 40971, Lot# L18U002). Fullerene soot is an rBC surrogate used for calibration of the SP2 due to its known density and similarities to ambient rBC (Baumgardner et al., 2012; Laborde et al., 2012). Data analysis was performed with the Paul Scherrer Institut Toolkit (PSI, Martin Gysel) developed for SP2 analysis within Igor Pro (Wavemetrics, Inc.).

2.3 Collection efficiency of the HR-ToF-AMS

In order to provide quantitative data from HR-ToF-AMS measurements, the particle collection efficiency (CE), which is largely due to particles bouncing on the vaporizer, needs to be evaluated. For the bypass line, we calculated the CE based on the composition-dependent algorithm proposed by Middlebrook et al. (2012) (i.e., CDCE). The CDCE for the bypass line ranges from 0.45 to 0.97, with the campaign-averaged value 0.52 ± 0.08 (one standard deviation). In order to validate the application of CDCE, we converted the mass concentrations of ambient non-refractory species measured by HR-ToF-AMS (after CDCE correction) together with the mass concentration of refractory species (i.e., rBC and crustal material) to volume using Eq. (45) and then compared the calculated volume with SMPS measurements.

$$\text{volume} = \frac{[\text{NO}_3^-] + [\text{SO}_4^{2-}] + [\text{NH}_4^+] + [\text{Cl}^-] + [\text{org}] + [\text{crustal material}] + [\text{BC}]}{1.75 + 1.52 \rho_{\text{org}} + 2.7 + 0.73} \quad \text{Eq. (45)}$$

In Eq. (45), 1.75 g cm^{-3} was used as the density for inorganic nitrate, sulfate, and ammonium, and 1.52 g cm^{-3} was used as the density for chloride (Poulain et al., 2014). The density of ambient organics was estimated using atomic O:C and H:C ratios as suggested by Kuwata et al. (2012). It is noted that the O:C and H:C ratios calculated based on Aiken et al. (2008) were used in the density estimation in order to be consistent with Kuwata et al. (2012). The organic density was estimated to be 1.30, 1.42 and 1.68 g cm^{-3} for bypass line, $\text{TD} = 120^\circ\text{C}$ and $\text{TD} = 250^\circ\text{C}$, respectively. The estimated density values were within the literature range (Hallquist et al., 2009). The concentration of crustal material was estimated by summing the normal oxides (Na_2O , MgO , Al_2O_3 , SiO_2 , CaO , K_2O , FeO , Fe_2O_3 , and TiO_2) of tracer elements (Malm et al., 1994). The tracer

elements were measured by PM_{1.0-0.3} rotating drum impactors and analyzed by synchrotron radiation-induced X-ray fluorescence spectrometry (Visser et al., 2015). The density of crustal material (2.7 g cm⁻³) was adapted from Lide (1991). The rBC concentration was measured by the SP2. For the rBC density, many previous studies have used 1.77 g cm⁻³ (Salcedo et al., 2006; Poulain et al., 2014; Huffman et al., 2009a). However, we note that 1.77 g cm⁻³ (adapted from Park et al. (2004)) is the inherent material density of diesel soot particles. If the inherent material density is used, one needs to consider the non-sphericity of rBC when comparing the calculated volume to the SMPS volume as the particles are assumed to be spherical when estimating the SMPS volume. In order to circumvent this issue, we used an effective density of rBC in this study. Park et al. (2003) measured the effective density of diesel soot particles in the 50-300nm range (mobility diameter) by using a Differential Mobility Analyzer - Aerosol Particle Mass analyzer (DMA - APM) system. The soot particles were firstly classified based on mobility diameter in DMA and the mass of classified particles was then measured by APM. The effective density was calculated with the following equation by assuming spherical particles:

$$\rho_{\text{eff}} = \frac{\text{mass}}{\frac{\pi}{6} d_{\text{me}}^3} \quad \rho_{\text{eff}} = \frac{\text{mass}}{\frac{\pi}{6} d_{\text{me}}^3} \quad \text{Eq. (26)}$$

where d_{me} is the mobility equivalent diameter. Thus, applying the effective density measured by a DMA-APM system allows one to convert BC mass to its apparent volume, which is comparable to the SMPS volume. One factor that complicates the choice of rBC effective density is that this value decreases with increasing mobility diameter as shown in Park et al. (2003). Limited by the lack of knowledge of the size distribution (mobility diameter based) of rBC in our data, we calculated the average effective density based on all the values reported in Park et al. (2003) and used this average value (0.73 g cm⁻³) in our study. This simplification is reasonable considering the following reasons. Firstly, Crilley et al. (2015) estimated that 70% of rBC at the Detling site is from traffic, which is similar to the BC types in Park et al. (2003). Secondly, the size distribution of total particles measured by SMPS in our study largely overlapped the size range studied in Park et al. (2003).

The calculated volume (based on HR-ToF-AMS + rBC + crustal material) was then compared with co-located SMPS measurements (Fig. 2). The SMPS measured the particle number distribution between 15.1 and 532.8 nm mobility diameter. The number distribution can be

converted to a volume distribution assuming spherical particles. On average, the difference between the calculated volume and the SMPS volume was within 6%, which validates the application of CDCE for the bypass line (Fig. 2a).

However, the CDCE is not applicable for the TD line because the CDCE algorithm is parameterized based on aerosol neutralization (Eq. (37)), which depends strongly on the accuracy of the ammonium concentration measurement. The ammonium concentration decreased quickly upon heating and was close to the instrument detection limit at 250°C. Thus, we evaluated the CE for the TD line by comparing the calculated volume (based on HR-ToF-AMS + rBC + crustal material) and the SMPS volume (Salcedo et al., 2006).

$$\text{neutralization} = \frac{\text{NH}_{4,\text{meas}}}{\text{NH}_{4,\text{predict}}} = \frac{\text{NH}_{4,\text{meas}}}{18 \times \left(\frac{\text{SO}_4 \times 2}{96} + \frac{\text{NO}_3}{62} + \frac{\text{Chl}}{35.5} \right)}$$

$$\text{neutralization} = \frac{\text{NH}_{4,\text{meas}}}{\text{NH}_{4,\text{predict}}} = \frac{\text{NH}_{4,\text{meas}}}{18 \times \left(\frac{\text{SO}_4 \times 2}{96} + \frac{\text{NO}_3}{62} + \frac{\text{Chl}}{35.5} \right)} \quad \text{Eq. (37)}$$

We noted that the selection of the rBC density has a substantial effect on the TD line CE. For example, varying the rBC density from 1.77 to 0.60 g cm⁻³ (i.e., from the inherent material density to the effective density of 100 nm diesel soot particle reported in Park et al. (2003)) changed the CE at 250°C by a factor of 2 (Table S1). This sensitivity analysis highlighted the importance of the rBC density in applying this method to evaluate CE, especially for the TD line where rBC accounted for a large fraction of the mass concentration. In this study, since the TD line CE calculated from Eq. (4) with an rBC effective density of 0.73 g cm⁻³ (i.e., average value from Park et al. (2003)) was close to the default value for CE (i.e., 0.45), we used 0.45 as the TD line CE in our analysis. As shown in Fig. 2b and 2c, the default CE results in a reasonable agreement between the calculated volume and the SMPS volume for the TD line. Specifically, the differences between the calculated volume and the SMPS volume are 14% and 11% at 120°C and 250°C, respectively, which are within the range of measurement uncertainties. Future studies are warranted to comprehensively investigate the change of AMS CE after heating of the aerosol.

2.3 Data analysis

2.3.1 Positive matrix factorization (PMF) analysis

Positive Matrix Factorization (PMF) analysis has been widely used for aerosol source apportionment in the AMS community. This technique represents the observed data as a linear combination of factors with constant mass spectra but varying concentrations across time in the dataset (Paatero and Tapper, 1994; Paatero, 1997). Two solvers have been used for PMF analysis of AMS data, PMF2 and the multilinear engine (ME-2). The PMF2 solver does not require a priori information, which avoids some subjectivity. The ME-2 solver uses a priori information to reduce rotational ambiguity among possible solutions (Canonaco et al., 2013; Paatero, 1999).

For the ambient OA measurements, we used the standard PMF2 solver, which does not include any a priori information. This analysis is denoted as PMF_{ambient} and was performed using the PMF Evaluation Toolkit (PET) software developed by Ulbrich et al. (2009). The error matrix was pre-treated based on the procedure in Ulbrich et al. (2009). m/z 's with signal-to-noise ratio in the range 0.2-2 were down weighted by a factor of 2, and m/z 's with signal-to-noise ratio smaller than 0.2 were removed. Also, the contributions of O^+ , HO^+ , H_2O^+ , CO^+ and CO_2^+ were down weighted to avoid excessive weighting of CO_2^+ and related fragments. Following the detailed procedure listed in Zhang et al. (2011), the PMF solutions were evaluated by investigating the key diagnostic plots (Fig. S4), mass spectral signatures, correlations with external tracers, and the diurnal profiles. The rotational ambiguity of the optimal solution was examined by changing the FPEAK parameter from -1 to 1. In our case, an FPEAK value of 0 ($Q/Q_{\text{exp}} = 1.804$) was selected because the correlations between factors and external tracers were not improved for FPEAK values that were different from 0. We resolved three factors from PMF_{ambient} , i.e., hydrocarbon-like OA (HOA), solid fuel OA (SFOA), and oxygenated OA (OOA), which are discussed in section 3.1. The choice of a three-factor solution is discussed in detail in the SI (Fig. S5).

For the TD line measurements, we first tried the PMF2 solver on the combined ambient and thermally-denuded OA spectra (denoted as $PMF_{\text{ambient+TD}}$); this is the same approach applied in Huffman et al. (2009a). However, in this study, we encountered several issues in $PMF_{\text{ambient+TD}}$ analysis. The first issue we encountered is the “mixing” behavior of OA factors. For example, in the three-factor solution of $PMF_{\text{ambient+TD}}$, one factor has similar fragmentation patterns as HOA from PMF_{ambient} , but this factor also has substantial signal at $C_2H_4O_2^+$ (m/z 60, often used as a

tracer marker for SFOA) (Fig. S6). In addition, another factor from $PMF_{\text{ambient}+\text{TD}}$ has similar time series as SFOA from PMF_{ambient} , but has similar mass spectrum as OOA from PMF_{ambient} . The second issue we encountered is that the mass loading of the OOA factor is occasionally higher in the TD runs compared to the preceding and succeeding bypass runs (Fig. S7). The reason for this behavior is not clear, but it is likely caused by the fact that only highly oxidized species remain upon heating and the mass spectrum of the remaining OA becomes more similar to the oxidized OA factors. Thus, PMF analysis might overestimate the concentrations of the oxidized OA factor. Overall, the PMF analysis on the combined bypass and TD line measurements by using the PMF2 solver without a priori information could not clearly separate OA factors. This is likely caused by the fact that including the thermally denuded data might distort the PMF results by introducing additional time variation in the mass spectra as pointed out by Huffman et al. (2009a).

Considering the above issues associated with $PMF_{\text{ambient}+\text{TD}}$, we performed PMF analysis using the ME-2 solver on the TD line measurements by applying the factor profiles determined from PMF_{ambient} as a priori information, in order to improve the separation of OA factor. Data obtained at 120°C and 250°C were analyzed separately in order to account for the variability of factor mass spectra at different temperatures. The analyses for 120°C and 250°C are denoted as ME-2_{120C} and ME-2_{250C}, respectively, and were performed using the toolkit Source Finder (SoFi v4.8) (Canonaco et al., 2013). The error matrix was pre-treated in the same way as for PMF_{ambient} . As recommended by Canonaco et al. (2013) and Crippa et al. (2014), secondary factors (i.e., OOA factor) were unconstrained and primary factors (i.e., HOA and SFOA) were constrained with a small a value (e.g., <0.1), which allows small variations of the resolved factors compared to the anchor profile in order to account for differences in ambient sources and avoid a mixing situation. We performed sensitivity tests and found that increasing the a value from 0 to 0.1 only reduced the fitting “residual” (i.e., Q/Q_{exp}) by <1% and had negligible influence on the factor profiles and factor concentrations (Figs. S8 and S9) for both ME-2_{120C} and ME-2_{250C}. Therefore, considering that 1) the small effect of the a value, and 2) the fact that the anchor profiles of HOA and SFOA resolved from PMF_{ambient} were clearly separated, we selected 0 as the a value, which fully constrained the profile of HOA and SFOA. The mass spectra of thermally-denuded OOA at 120°C and 250°C, which were not constrained in ME-2_{120C} and ME-2_{250C}, change slightly compared to the ambient OOA mass spectrum (Fig. S10). The most discernable changes occur at f_{CHO^+} (i.e.,

fraction of organic signal at CHO^+), $f_{\text{C}_2\text{H}_3\text{O}^+}$ and $f_{\text{CO}_2^+}$, suggesting that the composition of OOA is different at different denuding temperatures.

2.3.2 Retroplume analysis

Retroplume analysis was performed using the Numerical Atmospheric-Dispersion Modelling Environment (NAME) dispersion model (Jones et al., 2007) to identify the origin of air masses. The NAME model used the Unified Model reanalysis of meteorological data and generated the surface level pathways of air masses arriving at the site after 1 day of transport (i.e., 1-day footprints). The domain of influence of the NAME run was divided into a number of geographical regions (i.e., Atlantic ocean, Benelux area, etc, shown in Fig. S11) as described in Fleming et al. (2012). For each 3-hour period, the fraction of air masses arriving from each region was calculated. According to Liu et al. (2013), for the time periods when the fraction of one region is greater than the 40th percentile of that region's air masses fraction, that region is deemed to have a strong influence on the sampling site. Regions can also be grouped into broader sectors. In this study, we focused on two broader sectors, the easterly sector (North France and Benelux area) and the westerly sector (Atlantic and Ireland). It is important to note that sometimes the sampling site is influenced by more than one sector.

In the following discussion, we first investigate the PM_{10} composition and OA source apportionment at the Detling site (section 3.1). Then in section 3.2, we compare the measurements at the rural Detling site with the urban NK site to investigate the spatial variability of aerosol in the greater London area. Lastly, we examine the aerosol volatility based on measurements at the Detling site (section 3.3).

3 Results and Discussion

3.1 Aerosol characterization at the Detling site

Figure 3a shows the time series of PM_{10} composition measured by HR-ToF-AMS (i.e., non-refractory species) and SP2 (i.e., rBC). The campaign-average PM_{10} concentration is $14 \pm 12 \mu\text{g m}^{-3}$ (average \pm one standard deviation). The chemical composition of PM_{10} is dominated by nitrate and organics, which on average accounts for 32% and 31% of total PM_{10} mass, respectively. The other components include sulfate (17%), ammonium (14%), rBC (4.3%), and chloride (2.2%). Based on the fragmentation pattern of nitrate functionality in the AMS (i.e., $\text{NO}^+/\text{NO}_2^+$ ratio), one

can determine whether the nitrate is of organic or inorganic origin (Farmer et al., 2010; Boyd et al., 2015; Fry et al., 2009; Xu et al., 2015b). At the Detling site, the measured $\text{NO}^+/\text{NO}_2^+$ ratio is close to the value of pure ammonium nitrate (Fig. S12), indicating that the majority of the measured nitrates are inorganic nitrates.

The PMF analysis on the ambient organic mass spectra (i.e., $\text{PMF}_{\text{ambient}}$) resolves three OA subtypes: oxygenated organic aerosol (OOA), solid fuel organic aerosol (SFOA), and hydrocarbon-like organic aerosol (HOA), which accounts for 54%, 23%, and 19% of total OA, respectively. The time series and mass spectra of the three factors are shown in Fig. 4. HOA is representative of primary OA from vehicle emissions as its mass spectrum is dominated by hydrocarbon-like ions (i.e., C_xH_y^+ ions). HOA is correlated with rBC and NO_x (Fig. 4a). SFOA is a surrogate for fresh OA from solid fuel combustion, including biomass burning (Young et al., 2015b). The mass spectrum of SFOA is characterized by prominent signals at $\text{C}_2\text{H}_4\text{O}_2^+$ (m/z 60) and $\text{C}_3\text{H}_5\text{O}_2^+$ (m/z 73), which are likely fragments from anhydrosugars such as levoglucosan and mannosan (tracers for biomass burning). The time series of SFOA correlates with particle-phase nitrated phenol compounds (Mohr et al., 2013), which are mainly associated with coal and wood combustion (Fig. 4b). OOA is the most oxidized ($\text{O:C} = 0.92$) among all three factors. At the Detling site, the OOA time series shows a good correlation with sulfate (Pearson's $R=0.80$, Fig. 4a) and acetaldehyde ($R=0.78$, Fig. 4a). Acetaldehyde could arise from direct emissions, such as fossil fuel combustion and biomass burning, and secondary production by oxidation of various hydrocarbons (Langford et al., 2009). The observation that acetaldehyde correlates better with OOA than SFOA ($R = 0.78$ vs. 0.66) is consistent with previous studies which showed that acetaldehyde is dominated by secondary production after hours of photochemical processing (Hayes et al., 2013; Sommariva et al., 2011; de Gouw et al., 2005).

The identification of the sources of OOA is challenging because the mass spectrum of OA from different sources becomes more similar and resembles that of OOA with increasing photochemical aging (Ng et al., 2010; Jimenez et al., 2009). For the Detling data, we hypothesize that OOA is mainly from aged biomass burning. [Liu et al. \(2015\)](#) [Liu et al. \(2015\)](#) combined the PMF results from our study with radiocarbon analysis and estimated that 73-90% of carbon in the OOA factor was non-fossil. Biogenic emissions and biomass burning are the major sources for non-fossil carbon. The large fraction of non-fossil carbon indicates that the OOA measured at the Detling site largely arises from aged biomass burning because the concentration of biogenic VOCs

is low in winter due to cold temperature and reduced photosynthesis. For example, Yin et al. (2015) showed that the concentrations of isoprene SOA tracers (i.e., methyltetrols) and α -pinene SOA tracers (pinic acid and pinonic acid) at the NK site during the winter IOP are only 0.5 ng m^{-3} and 2.3 ng m^{-3} , respectively, which are substantially lower than the concentrations measured at US and European sites during warmer months. Both laboratory studies and ambient measurements have revealed that the oxidation of biomass burning OA is a rapid process (Hennigan et al., 2011; May et al., 2012; Bougiatioti et al., 2014; Zhao et al., 2015). During the oxidation process, the mass spectrum of biomass burning OA could lose its characteristic signature (i.e., $\text{C}_2\text{H}_4\text{O}_2^+$ and $\text{C}_3\text{H}_5\text{O}_2^+$) and becomes progressively similar to that of OOA (Grieshop et al., 2009a; Hennigan et al., 2011). Thus, the aged biomass burning OA could be apportioned to the OOA by PMF analysis. With this, it is possible that the biomass burning OA contributes a larger fraction of ambient OA in winter than what previous field studies suggested, where this factor was typically identified based on the presence of larger signals at $\text{C}_2\text{H}_4\text{O}_2^+$ (m/z 60) and $\text{C}_3\text{H}_5\text{O}_2^+$ (m/z 73) alone.

Figure 3b shows the aerosol composition when air masses come from the easterly sector (i.e., mainland Europe) and the westerly sector (i.e., Atlantic Ocean). The concentration of PM_{10} is five times higher for the easterly sector compared to the westerly sector. This is consistent with previous studies which showed that elevated pollution levels in the southern UK were often associated with heavily polluted air masses transported from mainland Europe (Charron et al., 2013; Morgan et al., 2010; Morgan et al., 2015; Putaud et al., 2004). Similar to the greater London area, Beekmann et al. (2015) found that 70% of fine PM in the Paris megacity was also largely influenced by regional contribution from mainland Europe. A large fraction of OA from mainland Europe is highly oxidized organic aerosol (i.e., OOA). For example, while the concentrations of HOA and SFOA only double when the source of air masses switches from the Atlantic Ocean to mainland Europe, the OOA concentration increases from $\sim 0.5 \text{ } \mu\text{g m}^{-3}$ to $\sim 3 \text{ } \mu\text{g m}^{-3}$ (Fig. 3b). The higher contribution of OOA to total OA is consistent with the total OA from mainland Europe being more oxidized than that from the Atlantic Ocean. In Fig. 5, we compare the OA oxidation level for different air masses in the f_{44} (i.e., fraction of organic signal at m/z 44) vs. f_{43} (i.e., fraction of organic signal at m/z 43) plot (Ng et al., 2010). The OA for the easterly sector has a higher f_{44} compared to the westerly sector, suggesting that the air masses advected from mainland Europe have undergone a larger extent of photochemical processing.

3.2 Comparison between London and Detling

In this section, we compare the two simultaneous HR-ToF-AMS measurements at the rural Detling site and the urban NK site. Only the sampling periods (hourly basis) when both instruments were operative from 20 January to 8 February, 2012 are included in the comparison, so that the concentrations reported in this section are different from those reported in section 3.1, where the whole data set at the Detling site (from 20 January to 15 February, 2012) is used.

3.2.1 Non-refractory species and OA factors comparison

The comparison between the Detling and NK sites in terms of concentration and diurnal variation of the five NR-PM₁ species is shown in Fig. 6 and Fig. S13, respectively. The concentration of nitrate is substantially higher at the urban NK site (i.e., 5.6 $\mu\text{g m}^{-3}$) than the rural Detling site (3.5 $\mu\text{g m}^{-3}$). This observation is consistent with McMeeking et al. (2012), who performed airborne measurements in the urban London region and observed an enhancement of nitrate concentration inside urban plumes. The elevated nitrate concentration (largely inorganic nitrate) at the urban site suggests that nitrate has a strong local contribution, likely due to the fact that nitrate formation occurs rapidly and its major sources (i.e., oxidation of NO_x) are much higher over inner London (Shaw et al., 2015). The sulfate concentration is well correlated between two sites ($R = 0.82$, Fig. 7), consistent with previous findings that sulfate has a strong regional contribution in the greater London area (Harrison et al., 2012; Yin et al., 2010). However, the sulfate concentration is about 60% higher at the rural Detling site than the urban NK site. The comparison of sulfate concentration between the rural and urban site depends on the origin of air masses. As shown in Fig. S14, the sulfate concentrations agree well between the two sites when air masses come from Atlantic Ocean (i.e., westerly) compared to mainland Europe (i.e., easterly). The reason for the elevated sulfate concentration at the rural site will be discussed below.

~~The sulfate concentration is well correlated between two sites ($R = 0.82$, Fig. 7), consistent with previous findings that sulfate has a strong regional contribution in the greater London area (Harrison et al., 2012; Yin et al., 2010). However, the sulfate concentration is about 60% higher at the rural Detling site than the urban NK site. The reasons for the elevated sulfate concentration at the rural site are unknown. Instrumental quantification may affect the comparison, but its role is expected to be minor. Although the two HR-ToF-AMS at the two sites were not compared side-by-side during the campaign, they agree well with the co-located instruments. For example, at the~~

Formatted: Font color: Auto

Formatted: Font color: Auto

Field Code Changed

Formatted: Font color: Auto

~~Detling site, the sulfate concentrations measured by the HR-ToF-AMS and SP-AMS (operated with laser off and tungsten vaporizer only) agree within 20%. In addition, the sulfate concentrations agree well between the two sites when air masses come from Atlantic Ocean (i.e., westerly) compared to mainland Europe (i.e., easterly) (Fig. S14), which implies that the higher sulfate concentration at the rural Detling site is not solely caused by instrumental quantification.~~

Although the average concentration of total OA is comparable between NK (i.e., $4.3 \mu\text{g m}^{-3}$) and Detling ($4.0 \mu\text{g m}^{-3}$) (Fig. 6), PMF analysis reveals that the ~~sources of contribution to total OA are largely from~~ different ~~for sources is distinctly different between the~~ urban and rural sites. At the urban NK site, primary OA sources, including cooking, vehicle emission, and solid fuel combustion, account for about 70% of total OA. At the rural Detling site, in contrast, more than half of the total OA is aged secondary OA (i.e., OOA). Specifically, the cooking OA (i.e., COA), which accounts for 18% of total OA at the urban NK site, is not resolved at the rural Detling site. This is expected as there is no cooking activity near the rural Detling site. Hydrocarbon-like OA (i.e., HOA) only shows weak correlation between the two sites ($R = 0.53$) (Fig. 8f), which is because HOA is representative of primary OA and it is influenced by local vehicle emissions. The SFOA time series is moderately correlated ($R = 0.65$) between Detling and NK (Fig. 8d). The SFOA concentration at the urban NK site is almost twice as high at the rural Detling site, which is likely due to the elevated domestic space heating activities and related emissions in the urban London area during wintertime (Young et al., 2015b; Crilley et al., 2015).

Among all three OA factors, the OOA factor has the strongest correlation between the two sites ($R = 0.81$) (Fig. 8b), which suggests that OOA likely represents regional SOA. Crilley et al. (2015) also observed that the filter-based daily-average OC concentration is well correlated ($R^2 > 0.82$) between Detling and NK sites during the same period as our study. However, the good correlations of OOA and OC observed in our study and Crilley et al. (2015) are different from the observation in Charron et al. (2013), where the authors found that secondary organic carbon (SOC) was much less spatially homogeneous than nitrate and sulfate by comparing an urban (Birmingham site) and a rural site (Harwell site) in the greater London area between July and November 2010. The difference between this study and Charron et al. (2013) is likely due to the uncertainty in the SOC estimation method. In Charron et al. (2013), SOC is estimated from filter measured total OC by using the EC/OC method where a constant EC/CC ratio from primary sources is applied. As discussed in Charron et al. (2013), their estimation and the weak correlation of OC between

Formatted: Font color: Auto

Formatted: Font color: Auto

Formatted: Font color: Auto

Formatted: Font color: Auto

Formatted: Font color: Auto

different sites are affected by the uncertainties associated with the choice of source ratios and analytical procedure. In addition to SOC estimation uncertainty, the differences in sampling sites, sampling periods, and size cuts (PM_{2.5} vs. PM₁) between Charron et al. (2013) and our study could also play a role.

Although the OOA is well-correlated between the two sites, the OOA concentration is almost twice as high at the rural Detling site than the urban NK site (Fig. 6). This observation is similar to the comparison of sulfate between the two sites, which is also usually considered to be regional, as discussed above. ~~The higher OOA concentration at the rural site is different from Zhang et al. (2007), who showed that the average OOA concentration is substantially lower at rural sites than urban sites.~~Based on atmospheric chemistry transport model, the higher OOA concentration at the rural site is a result of meteorological conditions, which cause a strong gradient of SOA concentration when air masses are advected from polluted mainland Europe. For example, to simulate the SOA formation in the winter IOP, Ots et al. (2015) applied the regional EMEP4UK (European Monitoring and Evaluation Programme) model, which uses 5 km by 5 km British Isles grid nested within 50 km by 50 km greater Europe domain, 21 vertical levels, Weather Research and Forecasting (WRF) model meteorological reanalysis, and National Atmospheric Emissions Inventory (NAEI) for the UK, Centre on Emission Inventories and Projections (CEIP) emissions for other European countries. They observed a steep negative gradient of SOA concentration from near European continent to southern England. The steep gradient is a result of meteorological conditions (i.e., mainly wind direction), which causes that the pollution plume from mainland Europe largely passes over the rural site, but not the urban site.

~~However, the trend reported in Zhang et al. (2007) is not based on simultaneous measurements at paired rural and urban sites. The reason for higher OOA concentration at the rural Detling site is unclear, but might be due to photochemical aging. For example, McMeeking et al. (2012) showed that OA/ Δ CO (i.e., Δ CO = measured CO – background CO) was substantially higher outside of the London plume compared to inside the plume, implying OA production occurred outside the plume. Considering the prevalent biomass burning in urban London and across Europe in winter (Young et al., 2015b; Crippa et al., 2014; Hellén et al., 2008; Fuller et al., 2013; Allan et al., 2010), higher OOA concentration at the rural Detling site may arise from the oxidation of emissions from biomass burning, which is in line with the observation that a large~~

Formatted: Font color: Auto

Field Code Changed

Formatted: Font color: Auto

Formatted: Font color: Auto

~~fraction of carbon in OOA is non fossil. However, further studies regarding the rural vs. urban comparison in winter are warranted to test the robustness of our observation.~~

3.2.2 OA oxidation level

Figure 5 compares the OA oxidation level between Detling and NK. Compared to the NK site, the average OA at the Detling site has higher f_{44} , indicating that the OA at the Detling site is more oxidized than that at the NK site. The difference in OA oxidation level between the Detling and the NK sites are due to different OA compositions. As shown in Fig. 6, the OA at the NK site is dominated by primary OA (~70% of total OA) from cooking, vehicle emissions, and solid fuel combustion, whose O:C is much lower than OOA. In contrast, more than half of OA at the Detling site is OOA, which is highly oxidized.

3.3 Aerosol volatility analysis

3.3.1 Volatility of non-refractory species and OA factors

~~Figure 9a shows and c show the thermograms and the change in concentration after heating (ΔC) of non-refractory (NR) species as measured by the HR-ToF-AMS. The mass fraction remaining (MFR) is calculated as the ratio of the species mass concentration through the TD to the average mass concentration of the preceding and succeeding bypass runs. The MFR has The ΔC is calculated as the concentration difference between the bypass and TD runs (Eq. (4)). Both the MFR and the ΔC have been corrected for the particle loss in the thermal denuder (TD) by using the TD transmission efficiency as discussed in section 2.2. The volatility MFR of NR species is consistent with previous ambient measurements (Huffman et al., 2009a). Nitrate is the most volatile has the largest average ΔC and the smallest MFR among all NR species. The MFR of nitrate decreases to 0.15 at 120°C and it volatilizes completely at 250°C (i.e., MFR < 0.05). Sulfate is the least volatile species at 120°C, with which has the smallest average ΔC and an MFR equal to 0.89. The sulfate MFR is higher than that of ammonium sulfate from laboratory studies, which has been attributed to particle mixing state affecting the sulfate volatility (Huffman et al., 2009a; Massoli et al., 2015). For OA, the MFR is about 0.16 at 250°C. On average, 0.88 $\mu\text{g m}^{-3}$ OA remains after heating, implying the existence of non-volatile organic compounds. As revealed by Figure 9d shows that the PMF analysis, the OOA factor ΔC 's of three OA factors are not statistically different at 120°C. This suggests that although the O:C of OOA (O:C = 0.92) has the lowest volatility among the three factors and accounts for 90% of the residual OA at 250°C (Fig.~~

Formatted: Font color: Auto

Formatted: Font color: Auto

Formatted: Font color: Auto

Formatted: Font color: Auto

Formatted: Font color: Auto

Formatted: Font color: Auto

Formatted: Font color: Auto

Formatted: Font color: Auto

~~9b). Theirs substantially larger than that of HOA (O:C = 0.22) and SFOA (O:C = 0.37), the volatilities of the three factors, which have are similar volatility at 120°C. Thus, the O:C may not be a good indicator of the volatility of the OA factors. At 250°C, both HOA and SFOA fully evaporate (MFR < 0.05) at 250°C so that the volatility cannot be compared under this temperature.~~

3.3.2 Sources of residual organics at 250°C

Figure 10 shows the chemical composition of the residual PM₁ after heating to 250°C. The major components of the residual PM₁ are OA (90% of OA is OOA), rBC, and sulfate. rBC accounts for about 30% of the remaining mass. This value is smaller than that reported in Poulain et al. (2014) (i.e., 47% in summer and 59% in winter for TD temperature 300°C) and in Häkkinen et al. (2012) (i.e., 55-87% depending on season for TD temperature 280°C). The differences are likely due to 1) the density of rBC used in previous studies when converting SMPS volume concentration to mass concentration, 2) different TD temperatures and residence times, 3) techniques to measure rBC concentration, and 4) sampling locations.

At 250°C, OA has the largest contribution (~40%) to the residual mass. The existence of highly oxidized, non-volatile organic compounds is consistent with previous ambient measurements and model studies. For example, Cappa and Jimenez (2010) used a kinetic model to simulate the volatility of OA factors measured by Huffman et al. (2009a) in the MILAGRO field campaign and the authors estimated that a large fraction of OA was non-volatile and would not evaporate under any atmospheric conditions.

The sources of non-volatile organics are uncertain, but appear to be related to anthropogenic emissions. A previous study by Häkkinen et al. (2012) showed that the MFR (excluding rBC) at 280°C correlated well with anthropogenic tracers (i.e., polycyclic aromatic hydrocarbons), indicating that the non-volatile species may be affected by anthropogenic emissions. In this study, we investigate the sources of the non-volatile organics by comparing the measurements of HR-ToF-AMS and SP-AMS after heating at 250°C. While the HR-ToF-AMS measures the bulk total non-refractory organics, SP-AMS only detects the organics associated with rBC when the SP-AMS is operated with the laser vaporizer only (i.e., no tungsten vaporizer) (Onasch et al., 2012). Figure 11 shows that after heating at 250°C, the residual organics associated with rBC correlate well with the residual organics in the bulk measurements, and they only account for <10% of the bulk measurements. Therefore, this good correlation is not caused by a large

Formatted: Font color: Auto

Formatted: Font color: Auto

Formatted: Font color: Auto

Formatted: Font color: Auto

Formatted: Font color: Auto

Formatted: Font color: Auto

contribution from rBC-associated species, but is possibly caused by the fact that the non-volatile organics in the bulk measurements have similar sources or have undergone similar chemical processing as rBC in the atmosphere. Denkenberger et al. (2007) suggested that the non-volatile organics may be oligomers formed within the TD based on the observation that oligomer intensity increased after heating ambient particles in a TD. In our study, the signals at high m/z (100 – 180), which are potential indicators for oligomers, decrease with TD temperature (Fig. S15). This suggests that the non-volatile organics are unlikely to be oligomers formed within the TD.

3.3.3 OA ~~volatility~~MFR and O:C ratio

To examine the relationship between O:C and ~~volatility~~MFR, the O:C of thermally-denuded OA is plotted as a function of TD temperature. As shown in Fig. 12a, the O:C of thermally-denuded OA increases with increasing TD temperature, indicating that the residual OA with lower volatility is more oxidized, which is consistent with previous observations (Huffman et al., 2009a; Huffman et al., 2009b). Thus, it appears that the OA oxidation level (i.e., O:C) is ~~inversely~~ correlated with ~~volatility~~MFR. If so, one would expect that ambient OA with higher O:C should have larger MFR. However, as shown in Fig. 12b to e, the MFR increases only slightly with the bypass O:C (or OS) over a wide range of O:C (or OS). In addition, the correlation between MFR and bypass O:C (or OS) is weak (i.e., $R < 0.4$), suggesting that the volatility of OA cannot be readily inferred by its O:C or OS.

The lack of correlation between OA MFR and O:C is likely due to the distributions of volatility and O:C in bulk OA, that is, one population of particles with a higher bulk O:C could have lower MFR after heating compared to another population of particles with a lower bulk O:C, if the volatility and O:C distributions are different between two populations. In the following discussion, we use a simple model to illustrate our point (Fig. 13). Two populations of particles are comprised of three compounds (i.e., A, B, and C), but with different amounts. These three compounds have the same molecular weight, but different volatility and O:C. The assumed properties of the three compounds and the compositions of two populations of particles are atmospherically relevant and are summarized in Fig. 13. Although the average O:C of population #2 (i.e., 0.75) is higher than that of population #1 (i.e., 0.61), population #2 has the same MFR as population #1 after heating, which is consistent with the trend in Fig. 12b-e. On the other hand, the O:C of each population always increases after heating, which is consistent with the observation in Fig. 12a. We note that the example described here is specific; however, it clearly illustrates that

the distributions of volatility and O:C largely influence the relationship between O:C and MFR of bulk OA. This also helps to explain the various types of relationship between O:C and MFR observed in laboratory studies (Grieshop et al., 2009b; Qi et al., 2010; Donahue et al., 2012; Kroll et al., 2009; Tritscher et al., 2011; Xu et al., 2014). In previous laboratory studies, while the SOA generally becomes progressively more oxidized (i.e., O:C increases) during the chemical aging, the volatility distribution evolves differently for different SOA systems, which results in various types of MFR trend (i.e., increases, or stays constant, or decreases over time). Our analysis emphasizes the importance of understanding the distribution of volatility and O:C in bulk OA and reveals the potential weakness of using one averaged O:C value to describe the degree of oxidation, which is in line with the two-dimensional volatility-oxidation modeling framework proposed by Donahue et al. (2011). In addition to the distribution of O:C and volatility, the fact that MFR depends on the initial concentration of OA, which is different between studies, may also contribute to the various relationships between O:C and MFR.

Hildebrandt et al. (2010) proposed that the lack of correlation between O:C and volatility in Finokalia, Greece was caused by the OA being highly oxidized with an average O:C of 0.8 (estimated from the measured f_{44}). In order to test this hypothesis, we plot the O:C enhancement (i.e., ratio between O:C of thermally denuded OA and O:C of ambient OA) vs. O:C of ambient OA (Fig. 14a) to show the O:C enhancement after heating. By extrapolating the linear fit under different temperatures, we find that if the O:C of ambient OA is about 1, the enhancement is negligible even after heating at 250°C. It is important to note that the O:C reported in Fig. 14a is calculated based on the recent formulation in Canagaratna et al. (2015). The improved O:C calculation method in Canagaratna et al. (2015) results in higher O:C compared to the values based on Aiken et al. (2008), which was used in Hildebrandt et al. (2010). By using the method in Aiken et al. (2008), we found that the O:C threshold for no enhancement is 0.8 (Fig. S16), which is the same as the O:C of ambient OA in Hildebrandt et al. (2010). In addition, the campaign-average f_{44} of ambient OA in Hildebrandt et al. (2010) is 0.182, which is close to f_{44} of TD OA under 250°C (i.e., 0.188) in our study (Fig. 14b). To conclude, this analysis provides a specific case in which the average O:C ratio might not be a good indicator of OA volatility.

4 Conclusions

In this study, we deployed a suite of instruments to characterize the composition of PM₁ at a rural site (Detling, Kent) near London during the Clean Air for London (ClearLo) project in 2012 winter. Nitrate and organics are two major components in PM₁, each of which accounts for ~30% of total PM₁ mass concentration. Retroplume analysis reveals that the PM₁ concentration in the greater London area is largely influenced by the origin of the air masses. When air masses are advected from mainland Europe, the PM₁ concentration is elevated and the organic aerosol is more oxidized. Oxygenated organic aerosol (OOA) accounts for ~50% of total OA. Taking advantage of measurements in winter when the biogenic emissions are low, we hypothesize that the OOA in the current study is likely aged OA from biomass burning. The hypothesis is based on the combined PMF and radiocarbon analysis where more than 70% of carbon in OOA is estimated to be non-fossil (Liu et al., 2015)(Liu et al., 2015) and cannot be explained by the small amount of biogenic SOA in winter.

With simultaneous HR-ToF-AMS measurements taking place at the rural Detling site and the urban North Kensington site, we have a unique opportunity to investigate the spatial variability of PM₁ in the greater London area. The nitrate concentration is markedly higher at the urban site compared to the rural site (i.e., 5.6 vs 3.5 µg m⁻³). The high nitrate concentration at the rural site together with the urban excess of nitrate imply that the nitrate in the greater London area has a high regional background overlaid by important contributions from local production. Although the OA concentration is comparable between the rural and urban sites, PMF analysis suggests distinctly different contribution from different sources of OA at between the two sites. Similar to previous studies, we find that OA at the urban site mainly arises from primary sources, while OA at the rural site is mainly secondary. Vehicle emission, solid fuel combustion, and cooking together account for ~70% of OA at the urban NK site. In contrast, OOA contributes more than half of total OA at the rural Detling site. Among all OA factors, OOA has the best correlation between the two sites (R = 0.81), which suggests that this factor is largely regional. We find that the OOA concentration is almost twice as high at the rural Detling site than the urban NK site. This is a result of meteorological conditions, which cause a strong gradient of SOA concentration when air masses are advected from polluted mainland Europe. The observation that the OOA concentration is higher at the rural site than urban site is opposite to the trend shown in Zhang et al. (2007).

Formatted: Font color: Auto

Formatted: Font color: Auto

Formatted: Font color: Auto

Formatted: Font color: Auto

~~However, the trend reported in Zhang et al. (2007) is not based on simultaneous measurements at paired rural and urban sites. The reason for the OOA excess at the rural Detling site is unclear, but might be related to photochemical aging of biomass burning emissions. Thus, our observation highlights the importance of meteorology in determining the OA spatial distribution.~~

Formatted: Font color: Auto

Field Code Changed

Formatted: Font color: Auto

Formatted: Font color: Auto

A TD was deployed to investigate the volatility of PM₁ species at the Detling site. We find that although OOA has substantial larger O:C than HOA and SFOA, the volatilities of these three factors are similar at 120°C, which is inferred from the change in mass concentration after heating at 120°C. This suggests that the O:C may not be a good proxy of OA factor volatility. We note that 16% of total OA remains even after heating at 250°C, suggesting the existence of non-volatile organics. PMF analysis reveals that the majority of the remaining organics are oxygenated OA. At 250°C, the time series of the residual organics measured by HR-ToF-AMS correlate well with the residual organics associated with rBC measured by SP-AMS. The good correlation suggests that the non-volatile organics likely have similar sources or have undergone similar chemical processing as rBC in the atmosphere, considering that rBC-associated organics only account for <10% of bulk organics.

Formatted: Font color: Auto

We evaluate the relationship between the volatility (using the MFR) and degree of oxidation (using the O:C or OS) of bulk OA. We found that, on the one hand, the O:C of thermally denuded OA is higher than that of ambient OA, indicating that less-volatile compounds have higher O:C. On the other hand, the MFR of OA shows a weak correlation with O:C of ambient OA, indicating that the average O:C of bulk OA may not be a good indicator for volatility. One possible explanation for the seemingly contradictory observations lies in the broad distribution of volatility and O:C in bulk OA. For example, different O:C distributions could result in the same bulk O:C but different volatility distributions, which may cause that particles with the same O:C to have different MFR. Thus, it is important to understand and use the distribution of properties (i.e., volatility and O:C) to describe the complexity of OA.

Acknowledgement

This project was supported by the US Department of Energy (grant no.DE-SC000602) and in part by the UK Natural Environment Research Council (NERC) ClearfLo project (grant ref. NE/H008136/1), coordinated by the National Centre for Atmospheric Science (NCAS). DEY acknowledges a NERC PhD studentship (ref. NE/I528142/1). ACA acknowledges Director's

postdoctoral funding from LANL's LDRD program. MKD acknowledges support by the US DOE Office of Biological and Environmental Research Atmospheric System Research Program, F265 to LANL. Elemental analysis was funded by the Swiss National Science Foundation (grant 200021_132467/1 and 200020_150056) and the European Community's Seventh Framework Programme (FP7/2007-2013, grant n°312284). The authors would like to thank the Met Office for use of the NAME dispersion model and the Meteorological data used in it and for the Leicester University ALICE supercomputer for running the model. The authors gratefully acknowledge Ashley Williamson (DOE), Amon Haruta (Los Alamos National Laboratory), David Green (Kings College London) and Roger Moore (Kent County Showgrounds) for assistance with the organization of the field site in Detling, UK. Processed and quality assured data are available through the ClearLo project archive at the British Atmospheric Data Centre (<http://badc.nerc.ac.uk/browse/badc/clearflo>) and through the US Department of Energy Atmospheric Radiation Measurement Archive (www.archive.arm.gov). Raw data are archived at the Georgia Institute of Technology and at Aerodyne Research, Inc. and are available on request.

Formatted: Font color: Auto

Formatted: Font color: Auto

References

Aiken, A. C., DeCarlo, P. F., and Jimenez, J. L.: Elemental Analysis of Organic Species with Electron Ionization High-Resolution Mass Spectrometry, *Anal Chem*, 79, 8350-8358, 10.1021/ac071150w, 2007.

Aiken, A. C., Decarlo, P. F., Kroll, J. H., Worsnop, D. R., Huffman, J. A., Docherty, K. S., Ulbrich, I. M., Mohr, C., Kimmel, J. R., Sueper, D., Sun, Y., Zhang, Q., Trimborn, A., Northway, M., Ziemann, P. J., Canagaratna, M. R., Onasch, T. B., Alfarra, M. R., Prevot, A. S. H., Dommen, J., Duplissy, J., Metzger, A., Baltensperger, U., and Jimenez, J. L.: O/C and OM/OC ratios of primary, secondary, and ambient organic aerosols with high-resolution time-of-flight aerosol mass spectrometry, *Environ Sci Technol*, 42, 4478-4485, Doi 10.1021/Es703009q, 2008.

~~Allan, J. D., Williams, P. I., Morgan, W. T., Martin, C. L., Flynn, M. J., Lee, J., Nemitz, E., Phillips, G. J., Gallagher, M. W., and Coe, H.: Contributions from transport, solid fuel burning and cooking to primary organic aerosols in two UK cities, *Atmos. Chem. Phys.*, 10, 647-668, 10.5194/acp-10-647-2010, 2010.~~

An, W. J., Pathak, R. K., Lee, B. H., and Pandis, S. N.: Aerosol volatility measurement using an improved thermodesorber: Application to secondary organic aerosol, *J Aerosol Sci*, 38, 305-314, DOI 10.1016/j.jaerosci.2006.12.002, 2007.

Baumgardner, D., Popovicheva, O., Allan, J., Bernardoni, V., Cao, J., Cavalli, F., Cozic, J., Diapouli, E., Eleftheriadis, K., Genberg, P. J., Gonzalez, C., Gysel, M., John, A., Kirchstetter, T. W., Kuhlbusch, T. A. J., Laborde, M., Lack, D., Muller, T., Niessner, R., Petzold, A., Piazzalunga, A., Putaud, J. P., Schwarz, J., Sheridan, P., Subramanian, R., Swietlicki, E., Valli, G., Vecchi, R., and Viana, M.: Soot reference materials for instrument calibration and intercomparisons: a workshop summary with recommendations, *Atmos Meas Tech*, 5, 1869-1887, DOI 10.5194/amt-5-1869-2012, 2012.

Beekmann, M., Prévôt, A. S. H., Drewnick, F., Sciare, J., Pandis, S. N., Denier van der Gon, H. A. C., Crippa, M., Freutel, F., Poulain, L., Gherzi, V., Rodriguez, E., Beirle, S., Zotter, P., von der Weiden-Reinmüller, S. L., Bressi, M., Fountoukis, C., Petetin, H., Szidat, S., Schneider, J., Rosso, A., El Haddad, I., Megaritis, A., Zhang, Q. J., Michoud, V., Slowik, J. G., Moukhtar, S., Kolmonen, P., Stohl, A., Eckhardt, S., Borbon, A., Gros, V., Marchand, N., Jaffrezo, J. L., Schwarzenboeck, A., Colomb, A., Wiedensohler, A., Borrmann, S., Lawrence, M., Baklanov, A., and Baltensperger, U.: In-situ, satellite measurement and model evidence ~~for a~~ **on the** dominant regional contribution to fine particulate matter levels in the Paris ~~Megacity~~ **megacity**, *Atmos. Chem. Phys. Discuss.*, 15, ~~8647-8686~~ **9577-9591**, 10.5194/~~aepd~~ **acp**-15-~~8647~~ **9577**-2015, 2015.

Bohnenstengel, S. I., Belcher, S. E., Aiken, A., Allan, J. D., Allen, G., Bacak, A., Bannan, T. J., Barlow, J. F., Beddows, D. C. S., Bloss, W. J., Booth, A. M., Chemel, C., Coceal, O., Di Marco, C. F., Dubey, M. K., Faloon, K. H., Fleming, Z. L., Furger, M., Gietl, J. K., Graves, R. R., Green, D. C., Grimmond, C. S. B., Halios, C. H., Hamilton, J. F., Harrison, R. M., Heal, M. R., Heard, D. E., Helfter, C., Herndon, S. C., Holmes, R. E., Hopkins, J. R., Jones, A. M., Kelly, F. J., Kotthaus, S., Langford, B., Lee, J. D., Leigh, R. J., Lewis, A. C., Lidster, R. T., Lopez-Hilfiker, F. D., McQuaid, J. B., Mohr, C., Monks, P. S., Nemitz, E., Ng, N. L., Percival, C. J., Prévôt, A. S. H., Ricketts, H. M. A., Sokhi, R., Stone, D., Thornton, J. A., Tremper, A. H., Valach, A. C., Visser, S., Whalley, L. K., Williams, L. R., Xu, L., Young, D. E., and Zotter, P.: Meteorology, Air Quality, and Health in London: The ClearfLo Project, *B Am Meteorol Soc*, 96, 779-804, 10.1175/BAMS-D-12-00245.1, 2014.

Bougiatioti, A., Stavroulas, I., Kostenidou, E., Zarnmpas, P., Theodosi, C., Kouvarakis, G., Canonaco, F., Prévôt, A. S. H., Nenes, A., Pandis, S. N., and Mihalopoulos, N.: Processing of biomass-burning aerosol in the eastern Mediterranean during summertime, *Atmos. Chem. Phys.*, 14, 4793-4807, 10.5194/acp-14-4793-2014, 2014.

Boyd, C. M., Sanchez, J., Xu, L., Eugene, A. J., Nah, T., Tuet, W. Y., Guzman, M. I., and Ng, N. L.: Secondary Organic Aerosol (SOA) formation from the β -pinene + NO₃ system: effect of humidity and peroxy radical fate, *Atmos. Chem. Phys. Discuss.*, 15, 2679-2744, 10.5194/acpd-15-2679-2015, 2015.

Canagaratna, M. R., Jayne, J. T., Jimenez, J. L., Allan, J. D., Alfarra, M. R., Zhang, Q., Onasch, T. B., Drewnick, F., Coe, H., Middlebrook, A., Delia, A., Williams, L. R., Trimborn, A. M., Northway, M. J., DeCarlo, P. F., Kolb, C. E., Davidovits, P., and Worsnop, D. R.: Chemical and

microphysical characterization of ambient aerosols with the aerodyne aerosol mass spectrometer, *Mass Spectrometry Reviews*, 26, 185-222, 10.1002/mas.20115, 2007.

Canagaratna, M. R., Jimenez, J. L., Kroll, J. H., Chen, Q., Kessler, S. H., Massoli, P., Hildebrandt Ruiz, L., Fortner, E., Williams, L. R., Wilson, K. R., Surratt, J. D., Donahue, N. M., Jayne, J. T., and Worsnop, D. R.: Elemental ratio measurements of organic compounds using aerosol mass spectrometry: characterization, improved calibration, and implications, *Atmos. Chem. Phys.*, 15, 253-272, 10.5194/acp-15-253-2015, 2015.

Canonaco, F., Crippa, M., Slowik, J. G., Baltensperger, U., and Prévôt, A. S. H.: SoFi, an IGOR-based interface for the efficient use of the generalized multilinear engine (ME-2) for the source apportionment: ME-2 application to aerosol mass spectrometer data, *Atmos. Meas. Tech.*, 6, 3649-3661, 10.5194/amt-6-3649-2013, 2013.

Cappa, C. D., and Jimenez, J. L.: Quantitative estimates of the volatility of ambient organic aerosol, *Atmos. Chem. Phys.*, 10, 5409-5424, 10.5194/acp-10-5409-2010, 2010.

Charron, A., Degrendele, C., Laongsri, B., and Harrison, R. M.: Receptor modelling of secondary and carbonaceous particulate matter at a southern UK site, *Atmos. Chem. Phys.*, 13, 1879-1894, 10.5194/acp-13-1879-2013, 2013.

Crilly, L. R., Bloss, W. J., Yin, J., Beddows, D. C. S., Harrison, R. M., Allan, J. D., Young, D. E., Flynn, M., Williams, P., Zotter, P., Prevot, A. S. H., Heal, M. R., Barlow, J. F., Halios, C. H., Lee, J. D., Szidat, S., and Mohr, C.: Sources and contributions of wood smoke during winter in London: assessing local and regional influences, *Atmos. Chem. Phys.*, 15, 3149-3171, 10.5194/acp-15-3149-2015, 2015.

Crippa, M., DeCarlo, P. F., Slowik, J. G., Mohr, C., Heringa, M. F., Chirico, R., Poulain, L., Freutel, F., Sciare, J., Cozic, J., Di Marco, C. F., Elsasser, M., Nicolas, J. B., Marchand, N., Abidi, E., Wiedensohler, A., Drewnick, F., Schneider, J., Borrmann, S., Nemitz, E., Zimmermann, R., Jaffrezo, J. L., Prévôt, A. S. H., and Baltensperger, U.: Wintertime aerosol chemical composition and source apportionment of the organic fraction in the metropolitan area of Paris, *Atmos. Chem. Phys.*, 13, 961-981, 10.5194/acp-13-961-2013, 2013.

Crippa, M., Canonaco, F., Lanz, V. A., Äijälä, M., Allan, J. D., Carbone, S., Capes, G., Ceburnis, D., Dall'Osto, M., Day, D. A., DeCarlo, P. F., Ehn, M., Eriksson, A., Freney, E., Hildebrandt Ruiz, L., Hillamo, R., Jimenez, J. L., Junninen, H., Kiendler-Scharr, A., Kortelainen, A. M., Kulmala, M., Laaksonen, A., Mensah, A. A., Mohr, C., Nemitz, E., O'Dowd, C., Ovadnevaite, J., Pandis, S. N., Petäjä, T., Poulain, L., Saarikoski, S., Sellegri, K., Swietlicki, E., Tiitta, P., Worsnop, D. R., Baltensperger, U., and Prévôt, A. S. H.: Organic aerosol components derived from 25 AMS data sets across Europe using a consistent ME-2 based source apportionment approach, *Atmos. Chem. Phys.*, 14, 6159-6176, 10.5194/acp-14-6159-2014, 2014.

de Gouw, J. A., Middlebrook, A. M., Warneke, C., Goldan, P. D., Kuster, W. C., Roberts, J. M., Fehsenfeld, F. C., Worsnop, D. R., Canagaratna, M. R., Pszenny, A. A. P., Keene, W. C., Marchewka, M., Bertman, S. B., and Bates, T. S.: Budget of organic carbon in a polluted atmosphere: Results from the New England Air Quality Study in 2002, *J Geophys Res-Atmos*, 110, Artn D16305 Doi 10.1029/2004jd005623, 2005.

DeCarlo, P. F., Kimmel, J. R., Trimborn, A., Northway, M. J., Jayne, J. T., Aiken, A. C., Gonin, M., Fuhrer, K., Horvath, T., Docherty, K. S., Worsnop, D. R., and Jimenez, J. L.: Field-Deployable, High-Resolution, Time-of-Flight Aerosol Mass Spectrometer, *Anal Chem*, 78, 8281-8289, 10.1021/ac061249n, 2006.

Denkenberger, K. A., Moffet, R. C., Holecek, J. C., Rebotier, T. P., and Prather, K. A.: Real-Time, Single-Particle Measurements of Oligomers in Aged Ambient Aerosol Particles, *Environ Sci Technol*, 41, 5439-5446, 10.1021/es070329l, 2007.

Donahue, N. M., Epstein, S. A., Pandis, S. N., and Robinson, A. L.: A two-dimensional volatility basis set: 1. organic-aerosol mixing thermodynamics, *Atmos. Chem. Phys.*, 11, 3303-3318, 10.5194/acp-11-3303-2011, 2011.

Donahue, N. M., Henry, K. M., Mentel, T. F., Kiendler-Scharr, A., Spindler, C., Bohn, B., Brauers, T., Dorn, H. P., Fuchs, H., Tillmann, R., Wahner, A., Saathoff, H., Naumann, K. H., Mohler, O., Leisner, T., Müller, L., Reining, M. C., Hoffmann, T., Salo, K., Hallquist, M., Frosch, M., Bilde, M., Tritscher, T., Barmet, P., Praplan, A. P., DeCarlo, P. F., Dommen, J., Prevot, A. S. H., and Baltensperger, U.: Aging of biogenic secondary organic aerosol via gas-phase OH radical reactions, *P Natl Acad Sci USA*, 109, 13503-13508, DOI 10.1073/pnas.1115186109, 2012.

Farmer, D. K., Matsunaga, A., Docherty, K. S., Surratt, J. D., Seinfeld, J. H., Ziemann, P. J., and Jimenez, J. L.: Response of an aerosol mass spectrometer to organonitrates and organosulfates and implications for atmospheric chemistry, *Proceedings of the National Academy of Sciences*, 107, 6670-6675, 10.1073/pnas.0912340107, 2010.

Fleming, Z. L., Monks, P. S., and Manning, A. J.: Review: Untangling the influence of air-mass history in interpreting observed atmospheric composition, *Atmos Res*, 104–105, 1-39, doi.org/10.1016/j.atmosres.2011.09.009, 2012.

Fry, J. L., Kiendler-Scharr, A., Rollins, A. W., Wooldridge, P. J., Brown, S. S., Fuchs, H., Dube, W., Mensah, A., dal Maso, M., Tillmann, R., Dorn, H. P., Brauers, T., and Cohen, R. C.: Organic nitrate and secondary organic aerosol yield from NO₃ oxidation of beta-pinene evaluated using a gas-phase kinetics/aerosol partitioning model, *Atmos Chem Phys*, 9, 1431-1449, 2009.

~~Fuller, G. W., Sciare, J., Lutz, M., Mouchtar, S., and Wagener, S.: New Directions: Time to tackle urban wood burning?, *Atmospheric Environment*, 68, 295-296, <http://dx.doi.org/10.1016/j.atmosenv.2012.11.045>, 2013.~~

Grieshop, A. P., Donahue, N. M., and Robinson, A. L.: Laboratory investigation of photochemical oxidation of organic aerosol from wood fires 2: analysis of aerosol mass spectrometer data, *Atmos. Chem. Phys.*, 9, 2227-2240, 10.5194/acp-9-2227-2009, 2009a.

Grieshop, A. P., Logue, J. M., Donahue, N. M., and Robinson, A. L.: Laboratory investigation of photochemical oxidation of organic aerosol from wood fires 1: measurement and simulation of organic aerosol evolution, *Atmos. Chem. Phys.*, 9, 1263-1277, 10.5194/acp-9-1263-2009, 2009b.

Häkkinen, S. A. K., Äijälä, M., Lehtipalo, K., Junninen, H., Backman, J., Virkkula, A., Nieminen, T., Vestenius, M., Hakola, H., Ehn, M., Worsnop, D. R., Kulmala, M., Petäjä, T., and Riipinen, I.: Long-term volatility measurements of submicron atmospheric aerosol in Hyttiälä, Finland, *Atmos. Chem. Phys.*, 12, 10771-10786, 10.5194/acp-12-10771-2012, 2012.

Hallquist, M., Wenger, J. C., Baltensperger, U., Rudich, Y., Simpson, D., Claeys, M., Dommen, J., Donahue, N. M., George, C., Goldstein, A. H., Hamilton, J. F., Herrmann, H., Hoffmann, T., Iinuma, Y., Jang, M., Jenkin, M. E., Jimenez, J. L., Kiendler-Scharr, A., Maenhaut, W., McFiggans, G., Mentel, T. F., Monod, A., Prevot, A. S. H., Seinfeld, J. H., Surratt, J. D., Szmigielski, R., and Wildt, J.: The formation, properties and impact of secondary organic aerosol: current and emerging issues, *Atmos Chem Phys*, 9, 5155-5236, 2009.

Harrison, R. M., Dall'Osto, M., Beddows, D. C. S., Thorpe, A. J., Bloss, W. J., Allan, J. D., Coe, H., Dorsey, J. R., Gallagher, M., Martin, C., Whitehead, J., Williams, P. I., Jones, R. L., Langridge, J. M., Benton, A. K., Ball, S. M., Langford, B., Hewitt, C. N., Davison, B., Martin, D., Petersson, K. F., Henshaw, S. J., White, I. R., Shallcross, D. E., Barlow, J. F., Dunbar, T., Davies, F., Nemitz, E., Phillips, G. J., Helfter, C., Di Marco, C. F., and Smith, S.: Atmospheric chemistry and physics in the atmosphere of a developed megacity (London): an overview of the REPARTEE experiment and its conclusions, *Atmos. Chem. Phys.*, 12, 3065-3114, 10.5194/acp-12-3065-2012, 2012.

Hayes, P. L., Ortega, A. M., Cubison, M. J., Froyd, K. D., Zhao, Y., Cliff, S. S., Hu, W. W., Toohey, D. W., Flynn, J. H., Lefer, B. L., Grossberg, N., Alvarez, S., Rappenglueck, B., Taylor, J. W., Allan, J. D., Holloway, J. S., Gilman, J. B., Kuster, W. C., De Gouw, J. A., Massoli, P., Zhang, X., Liu, J., Weber, R. J., Corrigan, A. L., Russell, L. M., Isaacman, G., Worton, D. R., Kreisberg, N. M., Goldstein, A. H., Thalman, R., Waxman, E. M., Volkamer, R., Lin, Y. H., Surratt, J. D., Kleindienst, T. E., Offenberg, J. H., Dusanter, S., Griffith, S., Stevens, P. S., Brioude, J., Angevine, W. M., and Jimenez, J. L.: Organic aerosol composition and sources in Pasadena, California, during the 2010 CalNex campaign, *J Geophys Res-Atmos*, 118, 9233-9257, Doi 10.1002/Jgrd.50530, 2013.

~~Hellén, H., Hakola, H., Haaparanta, S., Pietarila, H., and Kauhaniemi, M.: Influence of residential wood combustion on local air quality, *Sci Total Environ*, 393, 283-290, <http://dx.doi.org/10.1016/j.scitotenv.2008.01.019>, 2008.~~

Hennigan, C. J., Miracolo, M. A., Engelhart, G. J., May, A. A., Presto, A. A., Lee, T., Sullivan, A. P., McMeeking, G. R., Coe, H., Wold, C. E., Hao, W. M., Gilman, J. B., Kuster, W. C., de Gouw, J., Schichtel, B. A., Collett Jr, J. L., Kreidenweis, S. M., and Robinson, A. L.: Chemical and physical transformations of organic aerosol from the photo-oxidation of open biomass burning emissions in an environmental chamber, *Atmos. Chem. Phys.*, 11, 7669-7686, 10.5194/acp-11-7669-2011, 2011.

Hildebrandt, L., Engelhart, G. J., Mohr, C., Kostenidou, E., Lanz, V. A., Bougiatioti, A., DeCarlo, P. F., Prevot, A. S. H., Baltensperger, U., Mihalopoulos, N., Donahue, N. M., and Pandis, S. N.: Aged organic aerosol in the Eastern Mediterranean: the Finokalia Aerosol Measurement Experiment-2008, *Atmos Chem Phys*, 10, 4167-4186, DOI 10.5194/acp-10-4167-2010, 2010.

Hildebrandt Ruiz, L., Paciga, A. L., Cerully, K., Nenes, A., Donahue, N. M., and Pandis, S. N.: Aging of secondary organic aerosol from small aromatic VOCs: changes in chemical composition, mass yield, volatility and hygroscopicity, *Atmos. Chem. Phys. Discuss.*, 14, 31441-31481, 10.5194/acpd-14-31441-2014, 2014.

Huang, X. F., He, L. Y., Hu, M., Canagaratna, M. R., Sun, Y., Zhang, Q., Zhu, T., Xue, L., Zeng, L. W., Liu, X. G., Zhang, Y. H., Jayne, J. T., Ng, N. L., and Worsnop, D. R.: Highly time-resolved chemical characterization of atmospheric submicron particles during 2008 Beijing Olympic Games using an Aerodyne High-Resolution Aerosol Mass Spectrometer, *Atmos Chem Phys*, 10, 8933-8945, DOI 10.5194/acp-10-8933-2010, 2010.

Huffman, J. A., Ziemann, P. J., Jayne, J. T., Worsnop, D. R., and Jimenez, J. L.: Development and Characterization of a Fast-Stepping/Scanning Thermodenuder for Chemically-Resolved Aerosol Volatility Measurements, *Aerosol Sci Tech*, 42, 395-407, 10.1080/02786820802104981, 2008.

Huffman, J. A., Docherty, K. S., Aiken, A. C., Cubison, M. J., Ulbrich, I. M., DeCarlo, P. F., Sueper, D., Jayne, J. T., Worsnop, D. R., Ziemann, P. J., and Jimenez, J. L.: Chemically-resolved aerosol volatility measurements from two megacity field studies, *Atmos Chem Phys*, 9, 7161-7182, 2009a.

Huffman, J. A., Docherty, K. S., Mohr, C., Cubison, M. J., Ulbrich, I. M., Ziemann, P. J., Onasch, T. B., and Jimenez, J. L.: Chemically-Resolved Volatility Measurements of Organic Aerosol from Different Sources, *Environ Sci Technol*, 43, 5351-5357, 10.1021/es803539d, 2009b.

Jimenez, J. L., Canagaratna, M. R., Donahue, N. M., Prevot, A. S. H., Zhang, Q., Kroll, J. H., DeCarlo, P. F., Allan, J. D., Coe, H., Ng, N. L., Aiken, A. C., Docherty, K. S., Ulbrich, I. M., Grieshop, A. P., Robinson, A. L., Duplissy, J., Smith, J. D., Wilson, K. R., Lanz, V. A., Hueglin, C., Sun, Y. L., Tian, J., Laaksonen, A., Raatikainen, T., Rautiainen, J., Vaattovaara, P., Ehn, M., Kulmala, M., Tomlinson, J. M., Collins, D. R., Cubison, M. J., Dunlea, E. J., Huffman, J. A., Onasch, T. B., Alfarra, M. R., Williams, P. I., Bower, K., Kondo, Y., Schneider, J., Drewnick, F., Borrmann, S., Weimer, S., Demerjian, K., Salcedo, D., Cottrell, L., Griffin, R., Takami, A.,

Miyoshi, T., Hatakeyama, S., Shimono, A., Sun, J. Y., Zhang, Y. M., Dzepina, K., Kimmel, J. R., Sueper, D., Jayne, J. T., Herndon, S. C., Trimborn, A. M., Williams, L. R., Wood, E. C., Middlebrook, A. M., Kolb, C. E., Baltensperger, U., and Worsnop, D. R.: Evolution of Organic Aerosols in the Atmosphere, *Science*, 326, 1525-1529, DOI 10.1126/science.1180353, 2009.

Jones, A., Thomson, D., Hort, M., and Devenish, B.: The U.K. Met Office's Next-Generation Atmospheric Dispersion Model, NAME III, in: *Air Pollution Modeling and Its Application XVII*, edited by: Borrego, C., and Norman, A.-L., Springer US, 580-589, 2007.

Jonsson, A. M., Hallquist, M., and Saathoff, H.: Volatility of secondary organic aerosols from the ozone initiated oxidation of alpha-pinene and limonene, *J Aerosol Sci*, 38, 843-852, DOI 10.1016/j.jaerosci.2007.06.008, 2007.

Kroll, J. H., Smith, J. D., Che, D. L., Kessler, S. H., Worsnop, D. R., and Wilson, K. R.: Measurement of fragmentation and functionalization pathways in the heterogeneous oxidation of oxidized organic aerosol, *Phys Chem Chem Phys*, 11, 8005-8014, Doi 10.1039/B905289e, 2009.

Kuwata, M., Zorn, S. R., and Martin, S. T.: Using Elemental Ratios to Predict the Density of Organic Material Composed of Carbon, Hydrogen, and Oxygen, *Environ Sci Technol*, 46, 787-794, 10.1021/es202525q, 2012.

Laborde, M., Mertes, P., Zieger, P., Dommen, J., Baltensperger, U., and Gysel, M.: Sensitivity of the Single Particle Soot Photometer to different black carbon types, *Atmos Meas Tech*, 5, 1031-1043, DOI 10.5194/amt-5-1031-2012, 2012.

Langford, B., Davison, B., Nemitz, E., and Hewitt, C. N.: Mixing ratios and eddy covariance flux measurements of volatile organic compounds from an urban canopy (Manchester, UK), *Atmos. Chem. Phys.*, 9, 1971-1987, 10.5194/acp-9-1971-2009, 2009.

Lanz, V. A., Alfara, M. R., Baltensperger, U., Buchmann, B., Hueglin, C., and Prevot, A. S. H.: Source apportionment of submicron organic aerosols at an urban site by factor analytical modelling of aerosol mass spectra, *Atmos Chem Phys*, 7, 1503-1522, 2007.

Lee, B. H., Pierce, J. R., Engelhart, G. J., and Pandis, S. N.: Volatility of secondary organic aerosol from the ozonolysis of monoterpenes, *Atmospheric Environment*, 45, 2443-2452, DOI 10.1016/j.atmosenv.2011.02.004, 2011.

Lide, D. R.: *CRC Handbook of Chemistry and Physics*, CRC Press Inc, 1991.

Liu, D., Allan, J., Whitehead, J., Young, D., Flynn, M., Coe, H., McFiggans, G., Fleming, Z. L., and Bandy, B.: Ambient black carbon particle hygroscopic properties controlled by mixing state and composition, *Atmos. Chem. Phys.*, 13, 2015-2029, 10.5194/acp-13-2015-2013, 2013.

Liu, S., ~~A. C.~~ Aiken, A. C., Gorkowski, ~~K. J.~~, Dubey, M. K., Cappa, C. D., Williams, L. R., Herndon, S. C., Massoli, P., Fortner, E. C., Chhabra, P. S., Brooks, W. A., Onasch, T. B., Jayne, J. T., Worsnop, D. R., China, S., Sharma, N., Mazzoleni, C., Xu, L., Ng, N. L., Liu, D., Allan, J. D., Lee, J. D., Fleming, Z. L., Mohr, C., Zotter, P., Szidat, S., and Prevot, A. S. H.: Enhanced light absorption by mixed source black and brown carbon particles in UK winter, Submitted Nat Commun, 6, 10.1038/ncomms9435, 2015.

Malm, W. C., Sisler, J. F., Huffman, D., Eldred, R. A., and Cahill, T. A.: Spatial and seasonal trends in particle concentration and optical extinction in the United States, *Journal of Geophysical Research: Atmospheres*, 99, 1347-1370, 10.1029/93JD02916, 1994.

Massoli, P., Onasch, T. B., Cappa, C. D., Nuamaan, I., Hakala, J., Hayden, K., Li, S.-M., Sueper, D. T., Bates, T. S., Quinn, P. K., Jayne, J. T., and Worsnop, D. R.: Characterization of black carbon-containing particles from soot particle aerosol mass spectrometer measurements on the R/V Atlantis during CalNex 2010, *Journal of Geophysical Research: Atmospheres*, 120, 2575-2593, 10.1002/2014JD022834, 2015.

May, A. A., Saleh, R., Hennigan, C. J., Donahue, N. M., and Robinson, A. L.: Volatility of Organic Molecular Markers Used for Source Apportionment Analysis: Measurements and Implications for Atmospheric Lifetime, *Environ Sci Technol*, 46, 12435-12444, 10.1021/es302276t, 2012.

McMeeking, G. R., Bart, M., Chazette, P., Haywood, J. M., Hopkins, J. R., McQuaid, J. B., Morgan, W. T., Raut, J. C., Ryder, C. L., Savage, N., Turnbull, K., and Coe, H.: Airborne measurements of trace gases and aerosols over the London metropolitan region, *Atmos. Chem. Phys.*, 12, 5163-5187, 10.5194/acp-12-5163-2012, 2012.

Middlebrook, A. M., Bahreini, R., Jimenez, J. L., and Canagaratna, M. R.: Evaluation of Composition-Dependent Collection Efficiencies for the Aerodyne Aerosol Mass Spectrometer using Field Data, *Aerosol Sci Tech*, 46, 258-271, Doi 10.1080/02786826.2011.620041, 2012.

Mohr, C., DeCarlo, P. F., Heringa, M. F., Chirico, R., Slowik, J. G., Richter, R., Reche, C., Alastuey, A., Querol, X., Seco, R., Peñuelas, J., Jiménez, J. L., Crippa, M., Zimmermann, R., Baltensperger, U., and Prévôt, A. S. H.: Identification and quantification of organic aerosol from cooking and other sources in Barcelona using aerosol mass spectrometer data, *Atmos. Chem. Phys.*, 12, 1649-1665, 10.5194/acp-12-1649-2012, 2012.

Mohr, C., Lopez-Hilfiker, F. D., Zotter, P., Prévôt, A. S. H., Xu, L., Ng, N. L., Herndon, S. C., Williams, L. R., Franklin, J. P., Zahniser, M. S., Worsnop, D. R., Knighton, W. B., Aiken, A. C., Gorkowski, K. J., Dubey, M. K., Allan, J. D., and Thornton, J. A.: Contribution of Nitrated Phenols to Wood Burning Brown Carbon Light Absorption in Detling, United Kingdom during Winter Time, *Environ Sci Technol*, 47, 6316-6324, 10.1021/es400683v, 2013.

Morgan, W. T., Allan, J. D., Bower, K. N., Highwood, E. J., Liu, D., McMeeking, G. R., Northway, M. J., Williams, P. I., Krejci, R., and Coe, H.: Airborne measurements of the spatial distribution of aerosol chemical composition across Europe and evolution of the organic fraction, *Atmos. Chem. Phys.*, 10, 4065-4083, 10.5194/acp-10-4065-2010, 2010.

Morgan, W. T., Ouyang, B., Allan, J. D., Aruffo, E., Di Carlo, P., Kennedy, O. J., Lowe, D., Flynn, M. J., Rosenberg, P. D., Williams, P. I., Jones, R., McFiggans, G. B., and Coe, H.: Influence of aerosol chemical composition on N₂O₅ uptake: airborne regional measurements in northwestern Europe, *Atmos. Chem. Phys.*, 15, 973-990, 10.5194/acp-15-973-2015, 2015.

Ng, N. L., Canagaratna, M. R., Zhang, Q., Jimenez, J. L., Tian, J., Ulbrich, I. M., Kroll, J. H., Docherty, K. S., Chhabra, P. S., Bahreini, R., Murphy, S. M., Seinfeld, J. H., Hildebrandt, L., Donahue, N. M., DeCarlo, P. F., Lanz, V. A., Prevot, A. S. H., Dinar, E., Rudich, Y., and Worsnop, D. R.: Organic aerosol components observed in Northern Hemispheric datasets from Aerosol Mass Spectrometry, *Atmos Chem Phys*, 10, 4625-4641, DOI 10.5194/acp-10-4625-2010, 2010.

Onasch, T. B., Trimborn, A., Fortner, E. C., Jayne, J. T., Kok, G. L., Williams, L. R., Davidovits, P., and Worsnop, D. R.: Soot Particle Aerosol Mass Spectrometer: Development, Validation, and Initial Application, *Aerosol Sci Tech*, 46, 804-817, 10.1080/02786826.2012.663948, 2012.

[Ots, R., Young, D. E., Vieno, M., Xu, L., Dunmore, R. E., Allan, J. D., Coe, H., Williams, L. R., Herndon, S. C., Ng, N. L., Hamilton, J. F., Bergström, R., Marco, C. D., Nemitz, E., Mackenzie, I. A., Kuenen, J. J. P., Green, D. C., Reis, S., and Heal, M. R. H.: Simulating secondary organic aerosol from missing diesel-related intermediate-volatility organic compound emissions during the Clean Air for London \(ClearLo\) campaign, Submitted to *Atmos. Chem. Phys.*, 2015.](#)

Paatero, P., and Tapper, U.: Positive Matrix Factorization - a Nonnegative Factor Model with Optimal Utilization of Error-Estimates of Data Values, *Environmetrics*, 5, 111-126, DOI 10.1002/env.3170050203, 1994.

Paatero, P.: A weighted non-negative least squares algorithm for three-way 'PARAFAC' factor analysis, *Chemometr Intell Lab*, 38, 223-242, Doi 10.1016/S0169-7439(97)00031-2, 1997.

Paatero, P.: The Multilinear Engine—A Table-Driven, Least Squares Program for Solving Multilinear Problems, Including the n-Way Parallel Factor Analysis Model, *Journal of Computational and Graphical Statistics*, 8, 854-888, 10.1080/10618600.1999.10474853, 1999.

[Paciga, A., Karnezi, E., Kostenidou, E., Hildebrandt, L., Psichoudaki, M., Engelhart, G. J., Lee, B. H., Crippa, M., Prévôt, A. S. H., Baltensperger, U., and Pandis, S. N.: Volatility of organic aerosol and its components in the Megacity of Paris, *Atmos. Chem. Phys. Discuss.*, 15, 22263-22289, 10.5194/acpd-15-22263-2015, 2015.](#)

Park, K., Cao, F., Kittelson, D. B., and McMurry, P. H.: Relationship between Particle Mass and Mobility for Diesel Exhaust Particles, *Environ Sci Technol*, 37, 577-583, 10.1021/es025960v, 2003.

Park, K., Kittelson, D., Zachariah, M., and McMurry, P.: Measurement of Inherent Material Density of Nanoparticle Agglomerates, *J Nanopart Res*, 6, 267-272, 10.1023/B:NANO.0000034657.71309.e6, 2004.

Poulain, L., Birmili, W., Canonaco, F., Crippa, M., Wu, Z. J., Nordmann, S., Spindler, G., Prévôt, A. S. H., Wiedensohler, A., and Herrmann, H.: Chemical mass balance of 300 °C non-volatile particles at the tropospheric research site Melpitz, Germany, *Atmos. Chem. Phys.*, 14, 10145-10162, 10.5194/acp-14-10145-2014, 2014.

Putaud, J.-P., Raes, F., Van Dingenen, R., Brüggemann, E., Facchini, M. C., Decesari, S., Fuzzi, S., Gehrig, R., Hüglin, C., Laj, P., Lorbeer, G., Maenhaut, W., Mihalopoulos, N., Müller, K., Querol, X., Rodriguez, S., Schneider, J., Spindler, G., Brink, H. t., Tørseth, K., and Wiedensohler, A.: A European aerosol phenomenology—2: chemical characteristics of particulate matter at kerbside, urban, rural and background sites in Europe, *Atmospheric Environment*, 38, 2579-2595, <http://dx.doi.org/10.1016/j.atmosenv.2004.01.041>, <http://dx.doi.org/10.1016/j.atmosenv.2004.01.041>, 2004.

Qi, L., Nakao, S., Malloy, Q., Warren, B., and Cocker, D. R.: Can secondary organic aerosol formed in an atmospheric simulation chamber continuously age?, *Atmospheric Environment*, 44, 2990-2996, DOI 10.1016/j.atmosenv.2010.05.020, 2010.

Riipinen, I., Pierce, J. R., Donahue, N. M., and Pandis, S. N.: Equilibration time scales of organic aerosol inside thermodenuders: Evaporation kinetics versus thermodynamics, *Atmospheric Environment*, 44, 597-607, <http://dx.doi.org/10.1016/j.atmosenv.2009.11.022>, <http://dx.doi.org/10.1016/j.atmosenv.2009.11.022>, 2010.

Salcedo, D., Onasch, T. B., Dzepina, K., Canagaratna, M. R., Zhang, Q., Huffman, J. A., DeCarlo, P. F., Jayne, J. T., Mortimer, P., Worsnop, D. R., Kolb, C. E., Johnson, K. S., Zuberi, B., Marr, L. C., Volkamer, R., Molina, L. T., Molina, M. J., Cardenas, B., Bernabé, R. M., Márquez, C., Gaffney, J. S., Marley, N. A., Laskin, A., Shutthanandan, V., Xie, Y., Brune, W., Leshner, R., Shirley, T., and Jimenez, J. L.: Characterization of ambient aerosols in Mexico City during the MCMA-2003 campaign with Aerosol Mass Spectrometry: results from the CENICA Supersite, *Atmos. Chem. Phys.*, 6, 925-946, 10.5194/acp-6-925-2006, 2006.

[Saleh, R., Khlystov, A., and Shihadeh, A.: Determination of Evaporation Coefficients of Ambient and Laboratory-Generated Semivolatile Organic Aerosols from Phase Equilibration Kinetics in a Thermodenuder. *Aerosol Sci Tech*. 46, 22-30, 10.1080/02786826.2011.602762. 2011a.](#)

[Saleh, R., Shihadeh, A., and Khlystov, A.: On transport phenomena and equilibration time scales in thermodenuders. Atmos. Meas. Tech., 4, 571-581, 10.5194/amt-4-571-2011, 2011b.](#)

Schwarz, J. P., Gao, R. S., Fahey, D. W., Thomson, D. S., Watts, L. A., Wilson, J. C., Reeves, J. M., Darbeheshti, M., Baumgardner, D. G., Kok, G. L., Chung, S. H., Schulz, M., Hendricks, J., Lauer, A., Karcher, B., Slowik, J. G., Rosenlof, K. H., Thompson, T. L., Langford, A. O., Loewenstein, M., and Aikin, K. C.: Single-particle measurements of midlatitude black carbon and light-scattering aerosols from the boundary layer to the lower stratosphere, *J Geophys Res-Atmos*, 111, Artn D16207

Doi 10.1029/2006jd007076, 2006.

Shaw, M. D., Lee, J. D., Davison, B., Vaughan, A., Purvis, R. M., Harvey, A., Lewis, A. C., and Hewitt, C. N.: Airborne determination of the temporo-spatial distribution of benzene, toluene, nitrogen oxides and ozone in the boundary layer across Greater London, UK, *Atmos. Chem. Phys.*, 15, 5083-5097, 10.5194/acp-15-5083-2015, 2015.

Sommariva, R., de Gouw, J. A., Trainer, M., Atlas, E., Goldan, P. D., Kuster, W. C., Warneke, C., and Fehsenfeld, F. C.: Emissions and photochemistry of oxygenated VOCs in urban plumes in the Northeastern United States, *Atmos. Chem. Phys.*, 11, 7081-7096, 10.5194/acp-11-7081-2011, 2011.

Stanier, C. O., Pathak, R. K., and Pandis, S. N.: Measurements of the volatility of aerosols from alpha-pinene ozonolysis, *Environ Sci Technol*, 41, 2756-2763, Doi 10.1021/Es0519280, 2007.

Stephens, M., Turner, N., and Sandberg, J.: Particle identification by laser-induced incandescence in a solid-state laser cavity, *Appl Optics*, 42, 3726-3736, Doi 10.1364/Ao.42.003726, 2003.

[Tang, M. J., Shiraiwa, M., Pöschl, U., Cox, R. A., and Kalberer, M.: Compilation and evaluation of gas phase diffusion coefficients of reactive trace gases in the atmosphere: Volume 2. Diffusivities of organic compounds, pressure-normalised mean free paths, and average Knudsen numbers for gas uptake calculations. Atmos. Chem. Phys., 15, 5585-5598, 10.5194/acp-15-5585-2015, 2015.](#)

Tritscher, T., Dommen, J., DeCarlo, P. F., Gysel, M., Barmet, P. B., Praplan, A. P., Weingartner, E., Prévôt, A. S. H., Riipinen, I., Donahue, N. M., and Baltensperger, U.: Volatility and hygroscopicity of aging secondary organic aerosol in a smog chamber, *Atmos. Chem. Phys.*, 11, 11477-11496, 10.5194/acp-11-11477-2011, 2011.

Ulbrich, I. M., Canagaratna, M. R., Zhang, Q., Worsnop, D. R., and Jimenez, J. L.: Interpretation of organic components from Positive Matrix Factorization of aerosol mass spectrometric data, *Atmos. Chem. Phys.*, 9, 2891-2918, 10.5194/acp-9-2891-2009, 2009.

Visser, S., Slowik, J. G., Furger, M., Zotter, P., Bukowiecki, N., Dressler, R., Flechsig, U., Appel, K., Green, D. C., Tremper, A. H., Young, D. E., Williams, P. I., Allan, J. D., Herndon, S. C., Williams, L. R., Mohr, C., Xu, L., Ng, N. L., Detournay, A., Barlow, J. F., Halios, C. H., Fleming, Z. L., Baltensperger, U., and Prévôt, A. S. H.: Kerb and urban increment of highly time-resolved trace elements in PM₁₀, PM_{2.5} and PM_{1.0} winter aerosol in London during ClearLo 2012, *Atmos. Chem. Phys.*, 15, 2367-2386, 10.5194/acp-15-2367-2015, 2015.

Williams, L., Herndon, S., Jayne, J., Freedman, A., Brooks, B., Franklin, J. P., Massoli, P., Fortner, E., Chhabra, P. S., Zahniser, M. S., Stark, H., canagaratna, M., Onasch, T., Worsnop, D., Ng, N. L., Xu, L., Knighton, B., Aiken, A., Gorkowski, K. J., Liu, S., Martin, A. T., Coulter, R., Lopez-Hilfiker, F. D., Mohr, C., Thornton, J., Visser, S., Furger, M., Zotter, P., and Prevot, A. S. H.: Characterization of black carbon containing particles in rural wintertime UK with an Aerodyne soot particle aerosol mass spectrometer (SP-AMS), *Atmos. Chem. Phys. Discuss.*, in preparation, 2015.

Xu, L., Kollman, M. S., Song, C., Shilling, J. E., and Ng, N. L.: Effects of NO_x on the Volatility of Secondary Organic Aerosol from Isoprene Photooxidation, *Environ Sci Technol*, 48, 2253-2262, 10.1021/es404842g, 2014.

Xu, L., Guo, H., Boyd, C. M., Klein, M., Bougiatioti, A., Cerully, K. M., Hite, J. R., Isaacman-VanWertz, G., Kreisberg, N. M., Knote, C., Olson, K., Koss, A., Goldstein, A. H., Hering, S. V., de Gouw, J., Baumann, K., Lee, S.-H., Nenes, A., Weber, R. J., and Ng, N. L.: Effects of anthropogenic emissions on aerosol formation from isoprene and monoterpenes in the southeastern United States, *Proceedings of the National Academy of Sciences*, 112, 37-42, 10.1073/pnas.1417609112, 2015a.

Xu, L., Suresh, S., Guo, H., Weber, R. J., and Ng, N. L.: Aerosol characterization over the southeastern United States using high resolution aerosol mass spectrometry: spatial and seasonal variation of aerosol composition, sources, and organic nitrates, *Atmos. Chem. Phys. Discuss.*, 15, 10479-10552, 10.5194/acpd-15-10479-2015, 2015b.

Yin, J., Harrison, R. M., Chen, Q., Rutter, A., and Schauer, J. J.: Source apportionment of fine particles at urban background and rural sites in the UK atmosphere, *Atmospheric Environment*, 44, 841-851, <http://dx.doi.org/10.1016/j.atmosenv.2009.11.026>; <http://dx.doi.org/10.1016/j.atmosenv.2009.11.026>, 2010.

Yin, J., Cumberland, S. A., Harrison, R. M., Allan, J., Young, D. E., Williams, P. I., and Coe, H.: Receptor modelling of fine particles in southern England using CMB including comparison with AMS-PMF factors, *Atmos. Chem. Phys.*, 15, 2139-2158, 10.5194/acp-15-2139-2015, 2015.

Young, D. E., Allan, J. D., Williams, P. I., Green, D. C., Flynn, M. J., Harrison, R. M., Yin, J., Gallagher, M. W., and Coe, H.: Investigating the annual behaviour of submicron secondary

inorganic and organic aerosols in London, *Atmos. Chem. Phys.*, 15, 6351-6366, 10.5194/acp-15-6351-2015, 2015a.

Young, D. E., Allan, J. D., Williams, P. I., Green, D. C., Harrison, R. M., Yin, J., Flynn, M. J., Gallagher, M. W., and Coe, H.: Investigating a two-component model of solid fuel organic aerosol in London: processes, PM1 contributions, and seasonality, *Atmos. Chem. Phys.*, 15, 2429-2443, 10.5194/acp-15-2429-2015, 2015b.

Zhang, Q., Jimenez, J. L., Canagaratna, M. R., Allan, J. D., Coe, H., Ulbrich, I., Alfarra, M. R., Takami, A., Middlebrook, A. M., Sun, Y. L., Dzepina, K., Dunlea, E., Docherty, K., DeCarlo, P. F., Salcedo, D., Onasch, T., Jayne, J. T., Miyoshi, T., Shimojo, A., Hatakeyama, S., Takegawa, N., Kondo, Y., Schneider, J., Drewnick, F., Borrmann, S., Weimer, S., Demerjian, K., Williams, P., Bower, K., Bahreini, R., Cottrell, L., Griffin, R. J., Rautiainen, J., Sun, J. Y., Zhang, Y. M., and Worsnop, D. R.: Ubiquity and dominance of oxygenated species in organic aerosols in anthropogenically-influenced Northern Hemisphere midlatitudes, *Geophysical Research Letters*, 34, Artn L13801 Doi 10.1029/2007gl029979, 2007.

Zhang, Q., Jimenez, J. L., Canagaratna, M. R., Ulbrich, I. M., Ng, N. L., Worsnop, D. R., and Sun, Y. L.: Understanding atmospheric organic aerosols via factor analysis of aerosol mass spectrometry: a review, *Anal Bioanal Chem*, 401, 3045-3067, DOI 10.1007/s00216-011-5355-y, 2011.

Zhao, R., Lee, A. K. Y., Huang, L., Li, X., Yang, F., and Abbatt, J. P. D.: Photochemical processing of aqueous atmospheric brown carbon, *Atmos. Chem. Phys.*, 15, 6087-6100, 10.5194/acp-15-6087-2015, 2015.

Figure Captions

Fig. 1. Geographical locations of the sampling sites (i.e., North Kensington and Detling) in this study. The region circled by the M25 motorway is the greater London area. The map is adapted from Google Maps.

Fig. 2. Scatter plot of converted volume (based on HR-ToF-AMS total + BC + crustal material) vs. the apparent volume estimated from SMPS measurement for (a) the bypass line and the TD line at (b) 120°C and (c) 250°C. The composition-dependent CE is applied to the bypass line HR-ToF-AMS measurements and CE = 0.45 is applied to the TD line HR-ToF-AMS measurements. The slopes and intercepts are obtained by orthogonal distance regression (ODR). The Pearson's R is obtained by linear least-squares fit.

Fig. 3. (a) Time series of non-refractory species and black carbon in addition to the flag waves of dominant air mass origin based on the NAME model. (b) Average concentration of non-refractory species, black carbon, and OA factors resolved by PMF analysis for the easterly sector, westerly sector, and the whole campaign. The unexplained mass by PMF analysis is less than 6% of total OA and not shown in the figure. The gap between 1/22 and 1/25 is due to a clogged instrument inlet.

Fig. 4. (a) Time series of OA factors resolved from the unconstrained PMF analysis on the ambient data (i.e. PMF_{ambient}) and corresponding external tracers. (b) Mass spectra of OA factors, which are colored by the ion type. The time series of total nitrated phenols is from Mohr et al. (2013).

Fig. 5. f_{44} vs. f_{43} for Detling and NK sites, as well as for the westerly sector and easterly sector of the Detling site. The dotted lines were adapted from Ng et al. (2010). The averages are sized by average organic loading. The error bars indicate one standard deviation. The average OA concentration at the Detling site is different from the value in Fig. 3 due to different sampling periods.

Fig. 6. Comparison between NK and Detling sites in terms of the campaign-averaged concentration and mass fraction of non-refractory species and OA factors. The unexplained mass by PMF analysis is less than 6% of total OA and not shown in the figure.

Fig. 7. Comparison of non-refractory species time series between NK and Detling sites. The intercept and slope are obtained by orthogonal distance regression. The Pearson's R is obtained by linear least-squares fit.

Fig. 8. Comparison of OA factors time series between NK and Detling sites. The intercept and slope are obtained by orthogonal distance regression. The Pearson's R is obtained by linear least-squares fit.

Fig. 9. Thermogram of (a) non-refractory species and (b) OA factors ~~resolved from~~ The change in mass concentration after heating in the unconstrained PMF analysis on the ambient data TD (i.e.

PMF_{ambient} - ΔC) of (c) non-refractory species and (d) OA factors. Error bars indicate one standard deviation. The average values are connected by lines to guide the eyes.

Fig. 10. Mass fraction of PM₁ species for bypass line and TD line (i.e., 120°C and 250°C). The mass fractions larger than 9% are labeled in the figure.

Fig. 11. Comparison between organics associated with rBC (measured by SP-AMS with laser vaporizer only) and the non-refractory organics in the bulk measurement (by HR-ToF-AMS) after heating at 250°C.

Fig. 12. (a) Organic mass fraction remaining (MFR) and O:C as a function of TD temperature; (b) – (e) organic MFR at 120°C and 250°C as a function of bypass line organic O:C and oxidation state.

Fig. 13. The properties (O:C and volatility) of three model compounds and the composition of two populations of particles used in the simple model to illustrate the relationship between bulk OA O:C and volatility. The O:C is 1, 0.5, and 0.1 for compound A, B, and C, respectively. Upon heating at temperature T₀, 50%, 65% and 100% of A, B, and C would evaporate. Population #1 is comprised of 0.25, 0.7, and 0.05 μg m⁻³ of A, B, and C, respectively, and population #2 is comprised of 0.7, 0.05, and 0.25 μg m⁻³ of A, B, and C, respectively.

Fig. 14. (a) O:C enhancement (i.e., ratio of TD line O:C to bypass line O:C) as a function of bypass line O:C. (b) Mass spectra of OA under different TD temperatures. The signals between *m/z* 45 and 99 are multiplied by 10 and the signals between *m/z* 100 and 150 are multiplied by 25 for clarity. The mass spectra are colored by the ion type in the same way as Fig. 4b.

Fig. 1



Fig. 2

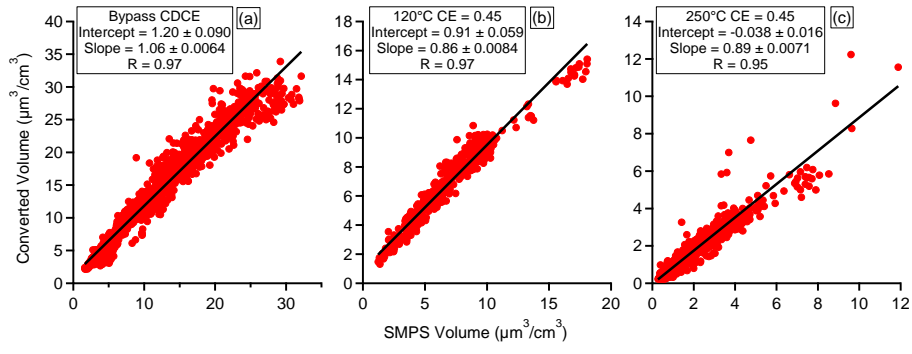


Fig. 3

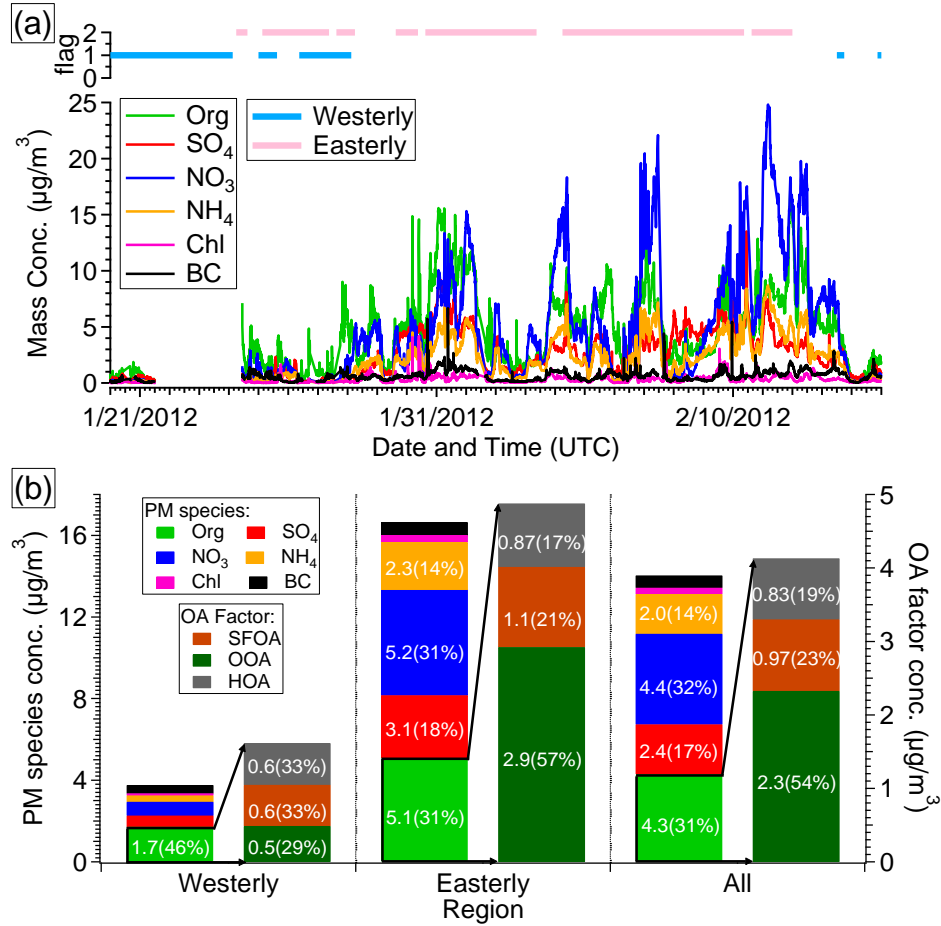
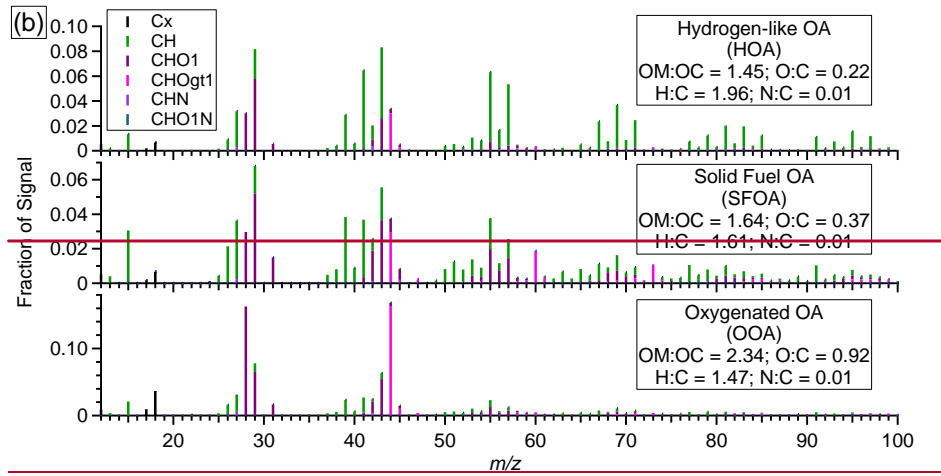
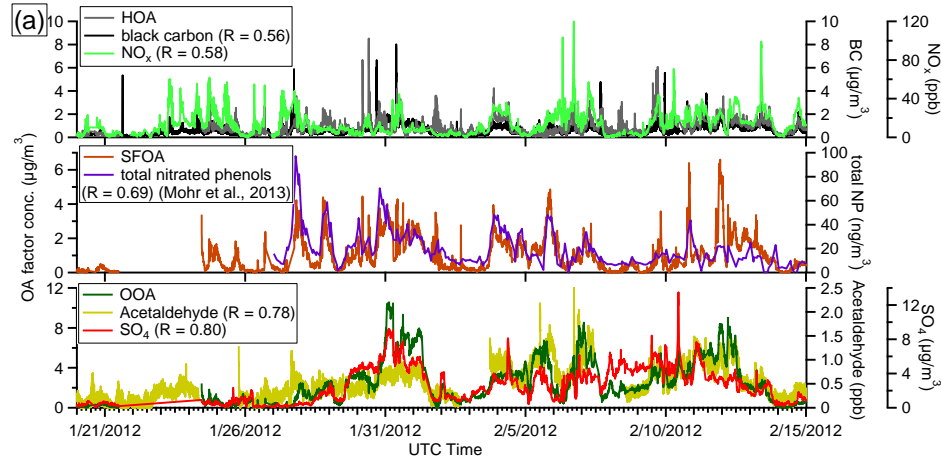


Fig. 4



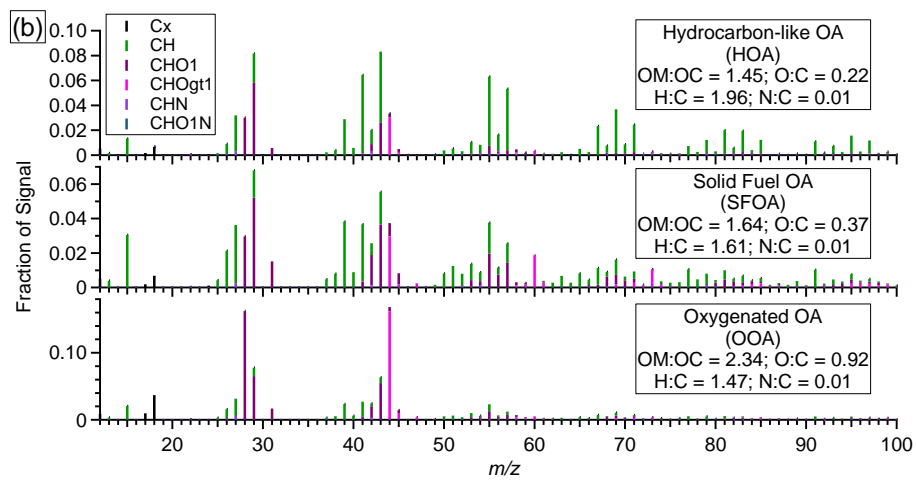


Fig. 5

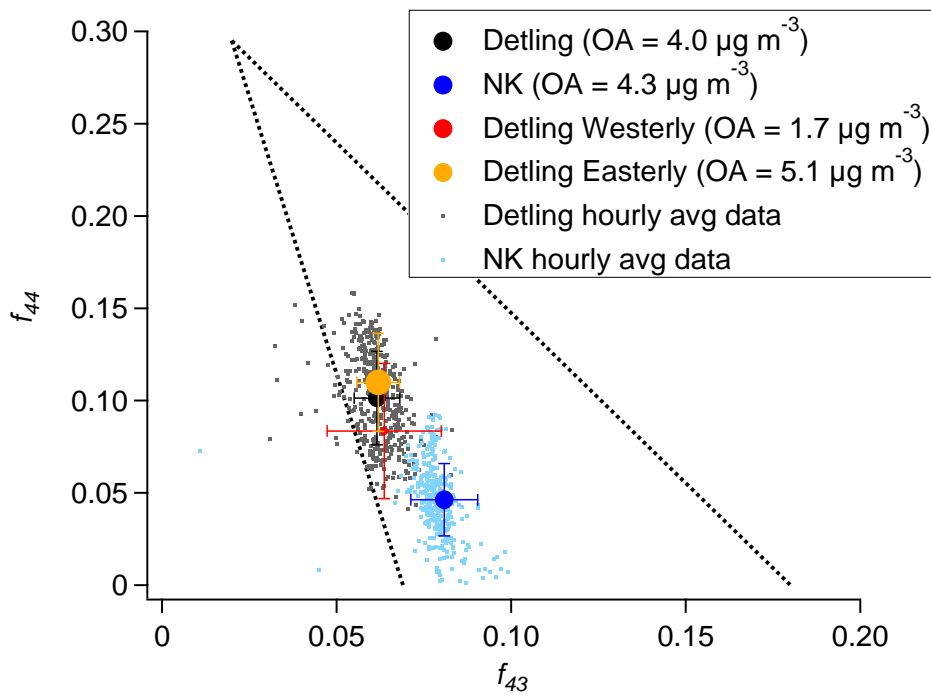


Fig. 6

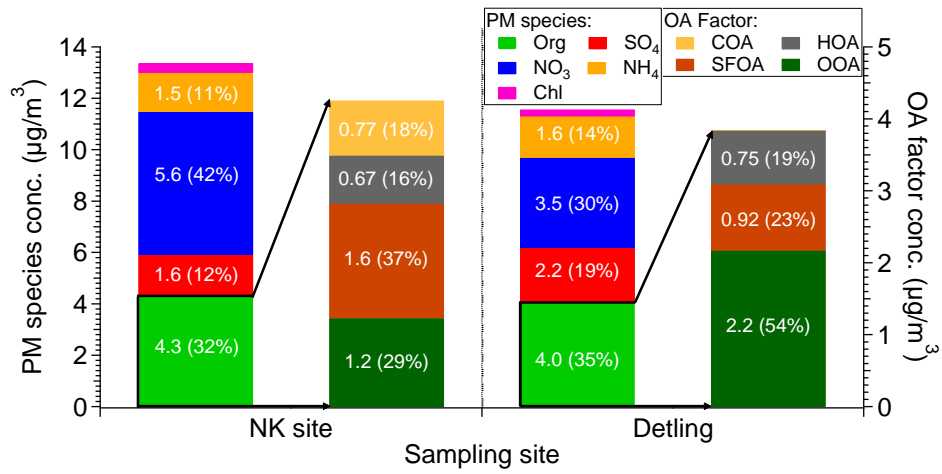


Fig. 7.

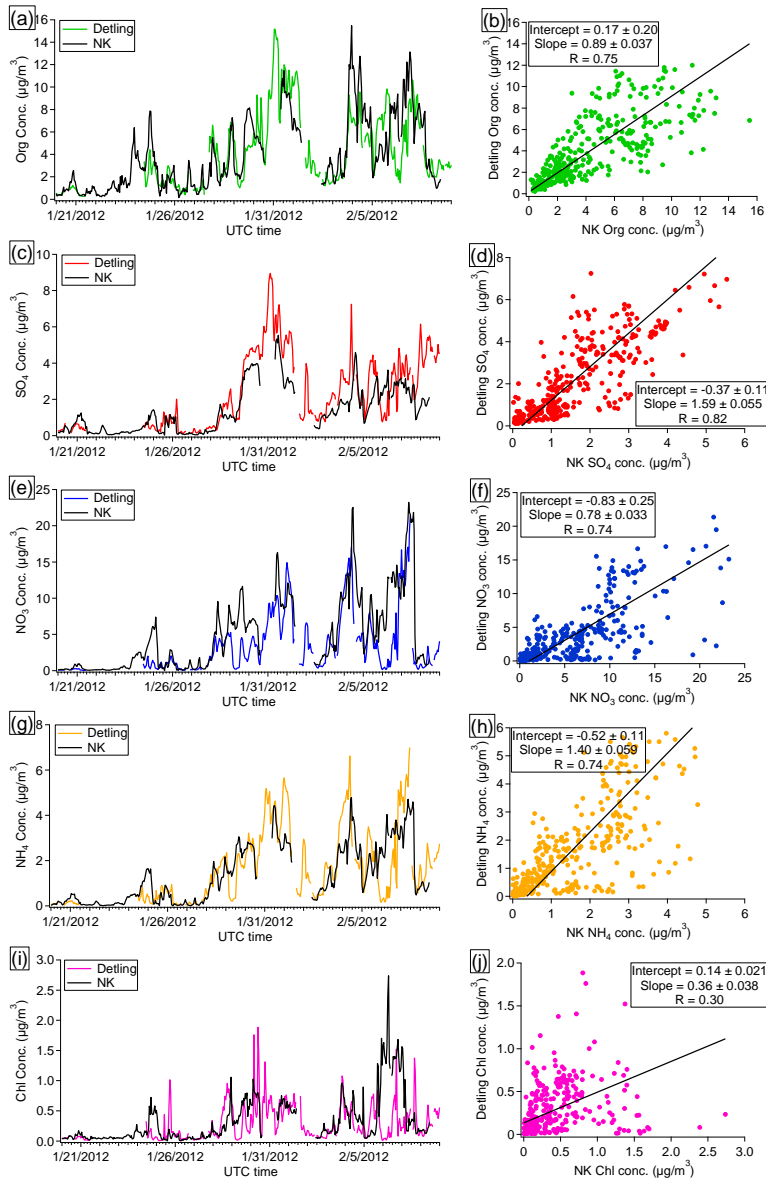


Fig. 8

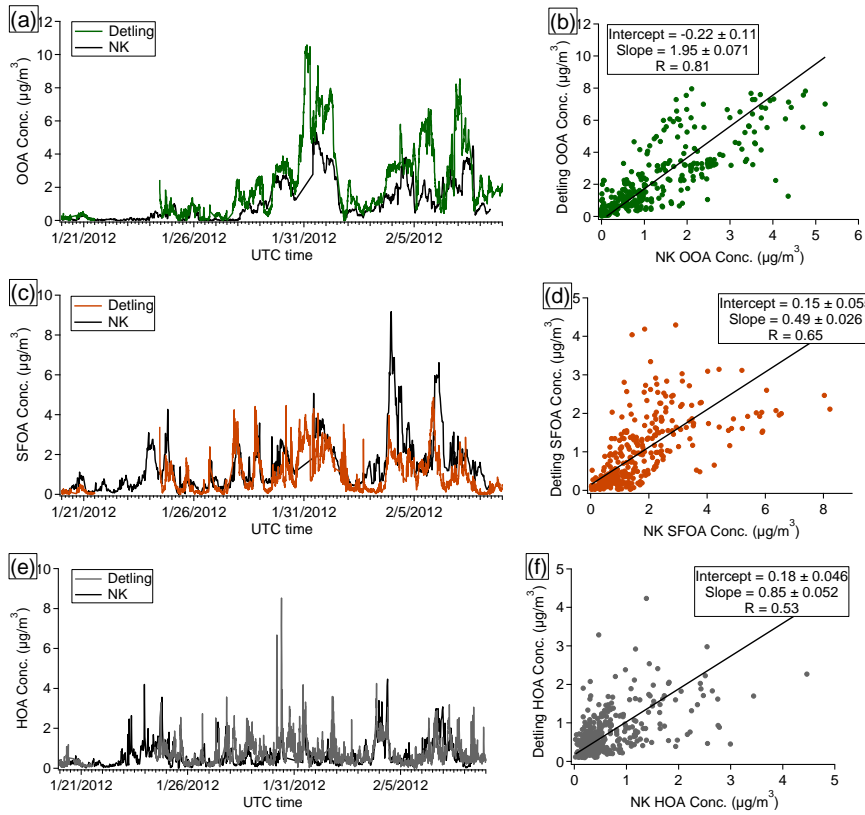
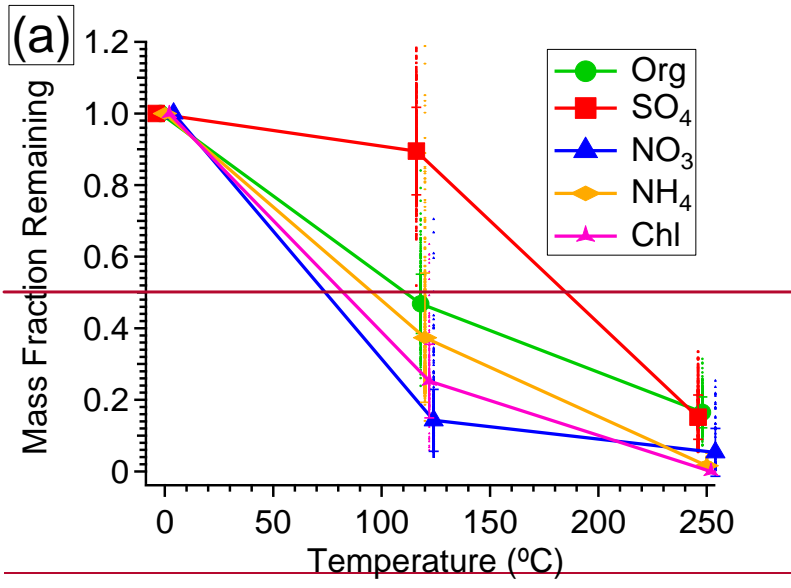
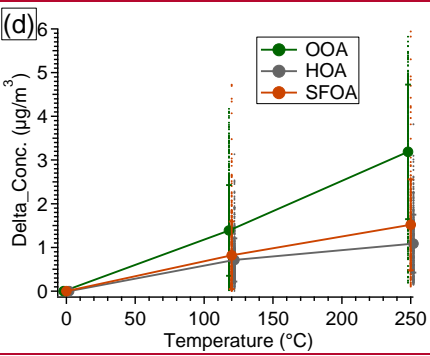
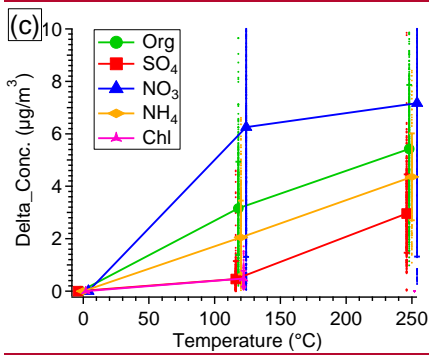
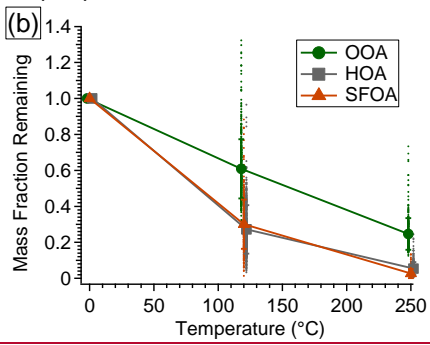
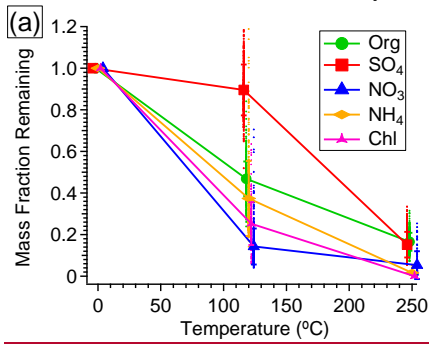
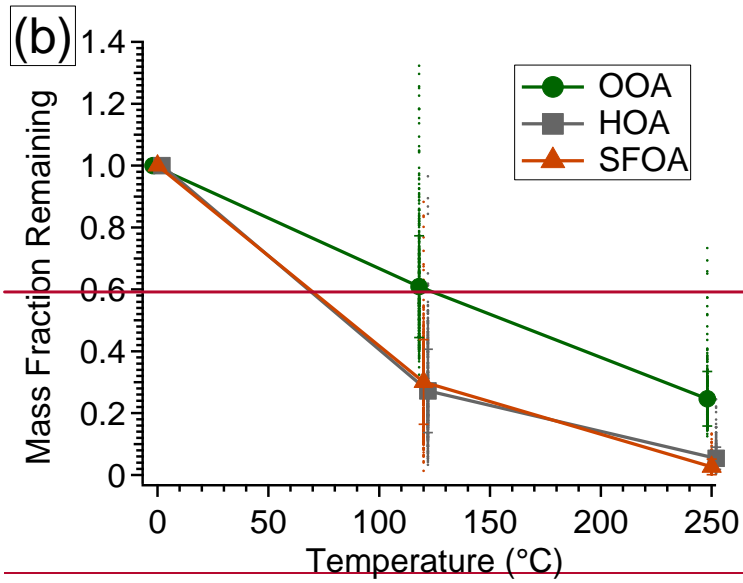


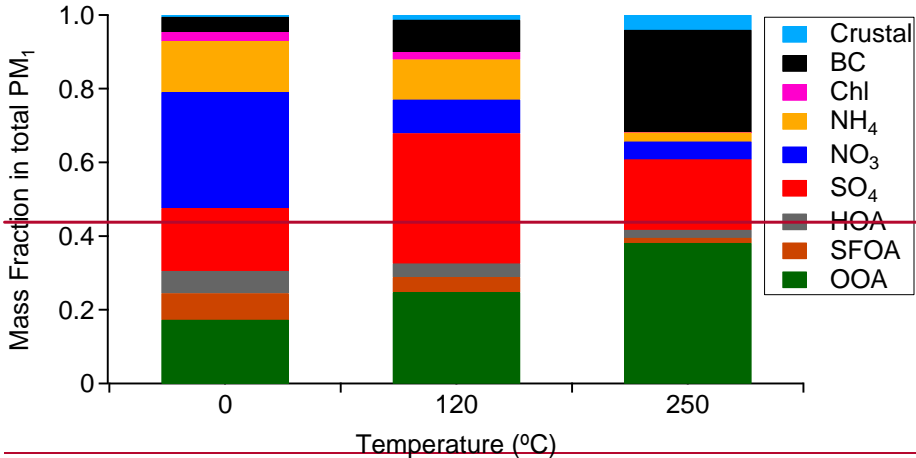
Fig. 9





Formatted: Justified

Fig. 10



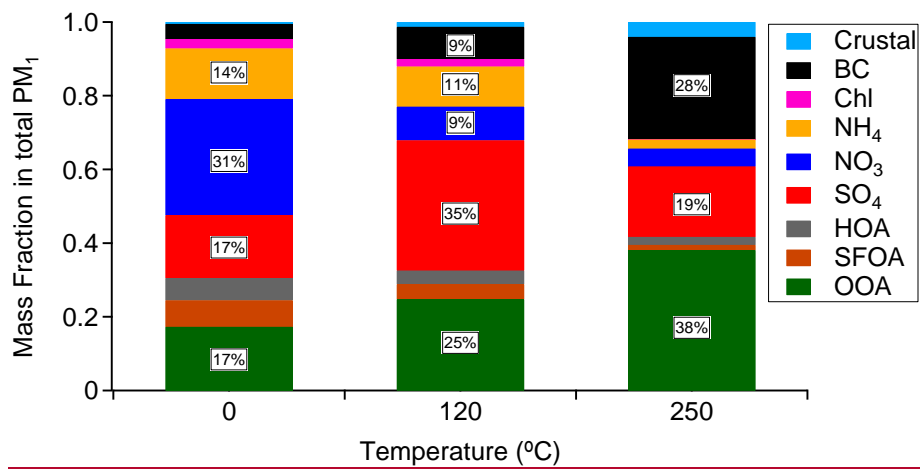


Fig. 11

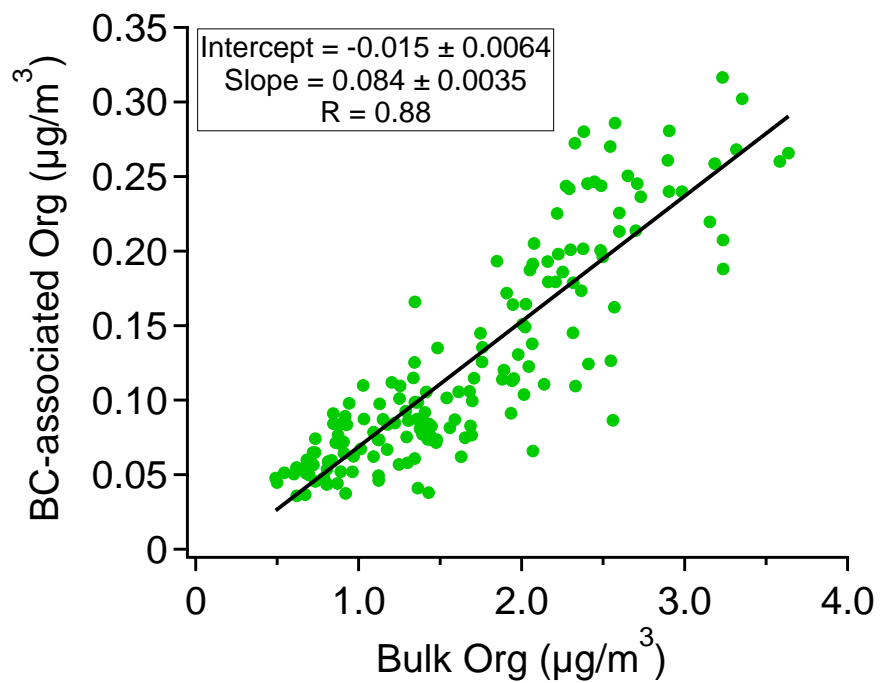


Fig. 12

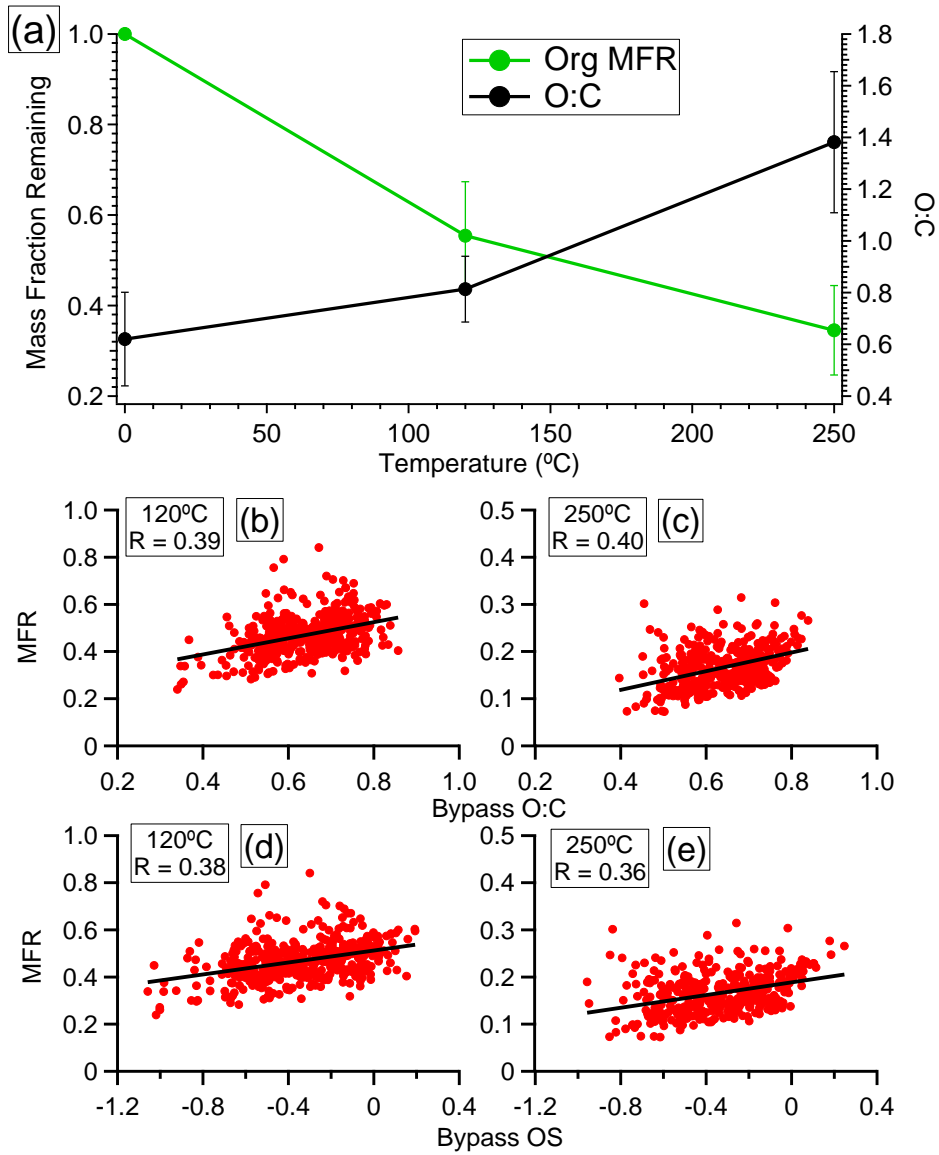


Fig. 13

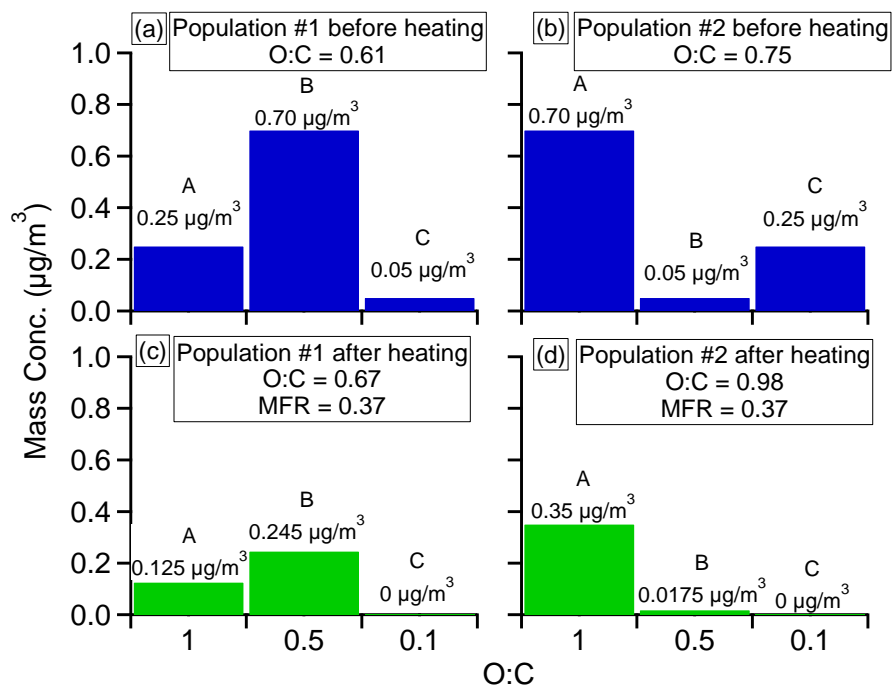


Fig. 14

